Journal of Power Sources 240 (2013) 421–441

Contents lists available at SciVerse ScienceDirect

Journal of Power Sources

journal homepage: www.elsevier.com/locate/jpowsour

Review

Review of the micro-tubular solid oxide fuel cell (Part II: Cell design issues and research activities)

V. Lawlor

Dept. Eco-Energy, Upper Austrian University of Applied Science, A-4600 Wels, Austria

HIGHLIGHTS

- Review presents state of the art MT-SOFC performance and manufacturing techniques.
- Cost considerations, geometry, material selection and architecture are reviewed.
- Possibilities for the manufacture of metal supported MT-SOFCs are discussed.
- Accounts of MT-SOFC performance with hydrocarbon fuels are presented.
- MT-SOFC durability and reliability requires more attention in the scientific literature.

ARTICLE INFO

Article history:
Received 27 August 2012
Received in revised form
26 February 2013
Accepted 2 March 2013
Available online 4 May 2013

Keywords:
Micro-tubular SOFC
Measurement
Simulation
Production
State of the art

ABSTRACT

Micro-Tubular Solid Oxide Fuel Cells (MT-SOFCs) are small tubular shaped, ceramic based, electrochemical electrical power generation devices that operate at high temperatures and can potentially be fuelled with hydrocarbon based fuels. In comparison to Part I of this review paper series, which considered stacks of MT-SOFCs, part II aims to gather and arrange information regarding MT-SOFCs, in order provide a state of the art account for those entering the field or those interested in the technology. This review paper deals with MT-SOFC; reported architectures, geometry and cost considerations, details regarding individual cell components, reported methods of producing MT-SOFCs, reports and details regarding MT-SOFCs and reforming, reported novel modes of operation, reports regarding the mechanical properties of MT-SOFCs, comment and reports regarding SOFC/MT-SOFC reliability and durability, and finally, comment and conclusions.

1. Introduction

1.1. SOFC/MT-SOFC technology

A Micro-Tubular Solid Oxide Fuel Cell (MT-SOFC) is a high-temperature fuel cell that electrochemically converts fuels, mainly those containing hydrogen in the compound, such as hydrocarbons, into electrical power. Fuel cell efficiency is ranked highly amongst various state of the art power providing technologies [1] and the SOFC is a technology that produces electricity remarkably efficiently [2]. However, the SOFC is distinguishable because these systems can achieve a very high system efficiency [3]. The high efficiency transpires when the SOFC's excess heat is used in order to drive additional turbines, to energise reformers or to heat water. Traditionally SOFCs and MT-SOFCs operated at 800–1000 °C, which complicates stack design and causes a narrower usable material base. Recently several groups [4–12] have reduced the SOFC's operating temperature to between 550 °C and 700 °C, while still achieving practical power densities, thus potentially simplifying stack design and augmenting the acceptable material base. However, operating at reduced temperatures hinders SOFC hydrocarbon reforming. In order to reform hydrocarbon fuels at reduced temperatures more expensive anode materials are required. Another option, should steam reforming be used, is to increase the steam to carbon ratio, which would reduce the SOFC fuel efficiency.

The SOFC accords three main advantages that other fuel cells do not afford. Firstly, a SOFC anode can permit internal hydrocarbon fuel reforming and not only tolerate but also even consume the reforming products [13–15]. Therefore, using fuels such as methane or syn-gas without a supplementary fuel reformer is conceivable under certain conditions [16]. Moreover, because low temperature fuel cells do not tolerate certain elements contained in the reformate, for example carbon monoxide in a PEM fuel cell,

E-mail address: vlawlor@gmail.com.

0378-7753/$ – see front matter © 2013 Elsevier B.V. All rights reserved.
http://dx.doi.org/10.1016/j.jpowsour.2013.03.191

often a single fuel reforming step is not adequate. Since lower temperature fuel cells cannot produce enough excess heat in order to energise a reformer an additional heat source that implies a parasitic system efficiency loss is necessitated. This furthermore complicates PEM and lower temperature operating fuel cell systems fed with hydrocarbons in comparison to SOFC systems.

Secondly, all fuel cells inherently produce heat from the electrochemical processes and various inherent resistances. SOFCs can produce excess heat of such a high potential that this heat reintegration into an overall system can allow meaningful peripheral tasks. For example, the excess heat energy can thermally self sustain the SOFC [17,18], power an integrated steam turbine and generator system [19–25], energise an endothermic reformer [26] or be accumulated in a medium such as water [27].

Finally, supplemental to the previous habitual SOFC attributes, the MT-SOFC extends the high-temperature SOFC's potential technological advantage and end product scope since it resides in much smaller geometric scale as compared to the standard planar and tubular SOFC classes. The small MT-SOFC's novelty is mainly its thermal shock resistance that allows a rapid start-up and increased power per volume when stacked [28], attributed to the large active surface to volume ratio.

1.2. Reported SOFC and MT-SOFC state of the art performances

SOFC stacks have been reported to provide as much as 85% fuel utilisation [29]. Simulation results of Chan et al. [30] showed that their SOFC-Gas Turbine power system could achieve a net electrical efficiency of better than 60% and a system efficiency (including waste heat recovery for steam generation) of better than 80%. Other reports regarding such high efficiencies for SOFC-gas turbine systems are found in Refs. [19–25]. Sidwell and Coors [31] have shown that peak electrical efficiency is always compromise between fuel utilisation and operating voltage, which act in opposition to each other. They concluded that it is possible to exceed 60% electrical efficiency in internally reforming SOFCs. Thus SOFCs internally reforming hydrocarbon based fuels are key to achieving the highest system efficiencies. The maximum reported electrical conversion efficiency for a SOFC system (3.1 kW) has been reported as 59% Direct Current Lower Heat Value (DC. LHV) [32], which it is claimed reached the world's highest level at the time of publication (2009). Recently, Watanabe et al. [33] have reported a MT-SOFC 700 W stack achieving an energy conversion efficiency of 47% (LHV) at 700 W output power with a fuel utilisation of 75%.

1.3. MT-SOFC application

In many cases application of MT-SOFC technology will be similar to the conventional SOFC technology. A current application, with several SOFC suppliers interested [34–36], is for truck APUs functioning as an alternative for engine idling. SOFCs have also been envisaged for Combined Heat and Power (CHP) in residential areas [24,37,38] and MT-SOFCs can also be used in such systems rather than the larger SOFC versions. Exciting applications for SOFCs are being envisaged for aircraft [39–41], automotive [42,43] and even submersible [44,45] application. The future for the MT-SOFC will be auspicious when the stacking and stack design problems are eradicated. For more information regarding MT-SOFCs the reader is pointed to Part I of this paper series [46] or to the review of Kendall [47]. For a well informed compacted introduction to key SOFCs aspects, with particular hydrocarbon use as fuel consideration, the reader is referred to the work of Kee et al. [48]. More detail regarding MT-SOFCs and hydrocarbon fuels are also provided in Section 5.

This review paper aims to gather and arrange information regarding MT-SOFCs in order facilitate those entering the field or those interested in the technology. Furthermore the paper should provide a state of the art account of the technology. The paper deals with MT-SOFC; reported architectures, geometry and cost considerations (Section 2), details regarding cell components (Section 3), reported methods of producing MT-SOFCs (Section 4), reports and details regarding MT-SOFCs and reforming (Section 5), reported novel modes of operation (Section 6), reports regarding the mechanical properties of MT-SOFCs (Section 7), comment and reports regarding SOFC/MT-SOFC reliability and durability (Section 8) and finally comment and conclusions (Section 9).

2. MT-SOFC materials: cost, design and geometry considerations

2.1. Introduction, costs and material consideration

The high-temperature fuel cell's operating principle is material dependent, necessitating ion or proton-conducting ceramics. Refs. [3,49–55] contain detailed information regarding SOFC materials. A very comprehensive paper by Wincewicz and Cooper [56] identified four anode material categories, five cathode material categories, four electrolyte material categories, and three categories highlighting interconnect materials. Electrolyte material consideration is governed by the SOFC operating temperature and its thickness, anode material consideration by its fuel compatibility and thermal expansion. Cathode material consideration is governed by its compatibility with the electrolyte, and finally, the interconnect material selection is determined by the SOFC operating temperature. Possible poisoning and thermal expansion should also be considered. Wincewicz and Cooper [56] provide charts in order to describe various SOFC manufacturing processes and in general the information is presented to the reader in a very informative way.

Published in 2007 the DOE/NETL report [57], pointed out that the SOFC material cost can vary quite a lot depending on the materials used. Contained in this report is a case study that analysed tubular cathode-supported and anode-supported stack construction cost. The raw material, material processing and manufacture costs were estimated and then combined in each case. Normally a tubular cathode-supported cell's material cost is expected to be higher than an anode-supported cell's material cost. A consequence of the thicker cathode $La_{0.8}Sr_{0.2}MnO_3$ (LSM) support, is that a lot of this relatively expensive material quantity is required in order to provide sufficient electrical conductivity and mechanical support. The case study found that economically the anode-supported cell's reduction in cathode size alleviation is offset by additional cost of silver, which was used as the electrical connection. They predicted that silver would account for between 25% and 50% of the overall anode-supported cell cost. The cathode material used in the case study was LSM. However, if more desirable cathode materials such as $La_{0.6}Sr_{0.4}Co_{0.2}Fe_{0.8}O_3$ (LSCF) or Sr-doped $LaFeO_3$ (LSF) had been considered, the cathode-supported cell would have been much more expensive. Highlighted by this study, is that the trade off between the current collector and cathode material in order to provide good electrical conduction becomes a very important economical consideration for SOFC mass production. In MT-SOFC related literature silver is predominately used as the cathode side current collector material. However, as indicated above other materials would significantly reduce a product's cost.

This study also reported that the manufacturing cost dominates a SOFCs products cost. However, the DOE/NETL report [56] does not provide MT-SOFC specific material or manufacturing process data. Regardless, much information that is applicable to MT-SOFC

material and production processes is documented. This data is relevant because, fundamentally, both the MT-SOFC and larger SOFC use the same materials and similar production processes. The MT-SOFC substrates are more suitably formed by processes such as extrusion and compression moulding, while tape casting for example is not yet suitable. More detail on MT-SOFC manufacture is discussed in Section 4.

2.2. Geometry and architecture

Standard MT-SOFCs are always reported as tubes as can be seen in Part I of this series [47] and with reference to reports listed in Table 1. In summary, MT-SOFCs are generally less than 1 cm in diameter. They are either cathode, electrolyte or anode supported with concentric tubular volumes that are consecutively sintered together. Various non-conventional MT-SOFC designs (i.e. not confined to concentric tubes as listed previously) are described in Finnerty and Coimbra [58] where anode geometry modifications are described. "Conventional"; refers to the support substrate being a standard tube. Fig. 1 shows examples patented by Finnerty and Coimbra [58]. These designs are suggested to provide mechanical, thermal, electrical and economic benefit. This is ascribed to combinations of the following; advantageous fuel flow distribution, increased active area, reduced current travelling paths and increased current collector contact area and, finally, less anode material. The use and the placement of fuel injector/current collect devices inside the anode hollow may also be facilitated in these designs. This would enable a counter flow inside the MT-SOFC as described in Ref. [59]. However, instead of the fuel manifold being sized or indeed altered in order to fit inside a conventional design [60], standard capillary pipes could be simply inserted, whereby the outlet flow through the cell would flow through the grooved channels in the anode.

Cathode-supported MT-SOFCs are a rather interesting case in the MT-SOFC field. Depending on the MT-SOFC foundation constituent, a MT-SOFC production price can vary significantly. Cathode materials are generally more expensive than anode and electrolyte materials [56]. Also since, for example, using a cathode or electrolyte support inhibits low temperature operation, careful preliminary material consideration is an indispensable MT-SOFC product design prerequisite [3]. Should the cathode form the MT-SOFC internal support component, an issue unique to the MT-SOFC field occurs. An internal cathode support implies that the electrolyte and anode can be added outside the tubular cathode substrate. This is easier than trying to apply these layers inside a narrow cathode tube substrate. However, if the cathode is the support structure, then the oxidant must flow through the tube and consequentially the air velocity is necessarily high. This may induce parasitic pressure losses. Indeed Luebbe et al. [61] have simulated this, to some degree, finding that as the cathode support gets thicker the concentration losses become almost exponentially higher.

Yamaguchi et al. [6] designed a novel micro-scale SOFC that had a cathode-supported honeycomb structure. The research was simulation-based and studied electrode area, pressure drop, and current collection modification in order to maximise the cell efficiency. The study results are summarised as follows; Firstly, they recommend that the cathode-honeycomb thickness should be less than 0.22 mm and the channel size should be more than 0.3 mm. These limits were recommended in order to ascertain sufficient electrode area and acceptable pressure drop facilitating a practical SOFC performance. Secondly, a simulation result indicated that short anode-supported cells ($<$2 mm) have a lower electrical resistance than honeycomb cathode-supported cells. However, once this length threshold is surpassed the situation is reversed. It is recommended that the anode-supported cells had non-linear electrical losses along their length while the honeycomb supported cells had linear losses. They fabricated a cathode-honeycomb supported SOFC with an impressive volumetric power density exceeding 1 W cm^{-3} at 650 °C.

Nether [62] modelled a novel unconventional cathode-supported MT-SOFC design incorporating multi cathode and anode direct connections along a MT-SOFCs length. Fig. 2 depicts the principle of Nether's [62] cascaded design. The cascaded MT-SOFC *I*/*V* characteristic indicated that high average voltages can be reached at low average current density. The transient simulation results showed a quick MT-SOFC power response when the load changed. This trait was observed for both the conventional MT-SOFC and cascaded concepts. During a load change, the minimum average cell voltages reached values of 0.67 V for the cascaded cell concept and 0.656 V for the conventional MT-SOFC. Nether [62] hypothesised that the cascaded MT-SOFC concept could work at higher load changes than the usual MT-SOFC design. However, regarding this concept, undesirable fuel and oxidant contamination would seem unpreventable. Normally the electrolyte should prevent fuel to oxidant and oxidant to fuel crossover. In this design a silver interconnector between the anode and cathode segments must also provide gas tightness. Funahashi et al. [63] also used a silver paste in order to maintain the fuel and oxidant isolation in regions where the electrolyte was removed. However, for commercial application silver may not be the ideal candidate for this task. Several reports have indicated that silver degrades when exposed to red-ox environments [64,65] over longer periods of time and furthermore it increases the costs [56].

To provide more information, some interesting MT-SOFC "stack designs" and electrical connections that build upon part I of this review [46] are discussed in the following; a crisscrossed stack design [66], a design similar to simple heat exchanger [67], a "cell encased in metal foam design" [68], various unconventional stacking designs [69], a multi tube cylindrical design including an exhaust gas combustor [70], a design with a porous metallic interconnect [71], a design with spines used as the interconnect [72], a segmented stack design [73] and a MT-SOFC based design with a unique geometry [74].

3. Specific detail regarding electrodes and electrolyte

3.1. The anode

As seen in Table 1 the majority of groups publishing works on MT-SOFCs tend to use the anode as the mechanical support. In such designs the anode is the largest component and this has import implications for the mechanical integrity. The MT-SOFC anode design may accord some additional benefit regarding mechanical robustness, see Section 7 for more detail. In general, both SOFC and MT-SOFC developers are concerned with the same anode related issues. This is because, fundamentally, the anode must perform the same function with the same materials for both designs.

Principally, the anode material must encompass both an ionic conductor and an electronic conductor that has an electro-catalytic property. The anode ionic conductor material is usually the electrolyte material, normally doped zirconia or ceria. In order to conduct the free electrons produced by the anode's fuel oxidation, the anode requires a metallic material such as nickel or copper in order to provide external circuit contact. This material is also expected to perform catalysis and oxidise the fuel while simultaneously conducting the freed electrons. Such a ceramic and metallic material combination is called a cermet. The composite anode material is then a heterogeneous mixed ionic and electronic conductor (HMIEC) [75]. There is a trade off between the amount of

Table 1
Table comparing the cell performance and attributes of different groups working in the MT-SOFC field.

General information			Electrolyte		Anode			Cathode			Cell characteristics				
Group	Support	Paper theme	Material	Thickness μm	Ohm cm^2	Mat/thick	Grain size	Ω cm^2	Mat/thick	Grain size	Ohmic resistance	W at 0.7 V	Operating temp	Fuel/oxidant	Inner/outer dia
Lawlor et al. [117]	ASC	Thermal analysis of a cell in cross-flow.	YSZ/GDC	10	Na	Ni/YSZ		Na	LSCF	Na	0.03 Ω cm^2	0.7 W cm^{-2}	987 K	100 ml min^{-1} 3% H_2O in H_2	1 mm 2.7 mm
Yamaguchi et al. [118]	CSC	Cathode-supported MT-SOFC with novel electrolyte and cathode materials. The oxidant was feed to the cell inside the tube.	Sc_2 O_2 doped YSZ	20	Na	c.a 3.5 μm	1 μm	6 Ω cm	LSM & LSM–GDC 400 μm &10 μm	2–3 and 1 μm	1.7 Ω cm^2 (OCV)	0.325 W cm^{-2}	1023 K	3% H_2O in H_2	1mm/2 mm
Yang et al. [119]	ASC	MT-SOFC made with phase inversion. Hollow fibre method.	YSZ/SDC	Ca. 10–20	Na	NiO/YSZ/SDC Ca. 300 μm	1.73 μm	Na	LSM/YZS/SDC	Na	0.42 Ω cm^2	1 W cm^{-2}	1073 K	35 ml min^{-1} 15% H_2O in H_2	1mm/ 1.5 mm
Campana et al. [120]	ASC	Thermal cycling of Mt-SOFCs and effect of cathode thickness and sintering temperature on cell performance	YSZ	Ca. 15–20	Na	Ni–YSZ	400 μm	LSM–YSZ	100, 50 μm	Na	0.293 Ω cm^2	0.7 a cm^2	1177 K	3% H_2O	2.4 mm I.D.
Calise et al. [121]	ASC	Testing of a MT-SOFC using a GDC ion conductor	GDC/	10	Na	Ni/GD	Ca. 250 μm	LSCF	Ca. 20 μm	Na	OCV 0.2 Ω cm^2	0.65 W cm^{-2}	823 K	25 ml min^{-1}	1.8 mm
Nakajima et al. [122]	ASC	Impedance to indicate temperature profile on a cell	LSGM	<30	Na	NiO/YSZ & NiO CGO	Na	LSCF	<30 μm	Na	0.2 Ω cm^2	0.28 W cm^{-2}	973 K	120 ml min^{-1} 50% N_2/H_2	3mm/5 mm
Galloway and Sammes [123]	ASC	Performance of cells in the intermediate range.	GDC	10	Na	NiO–GDC	Ca. 250 μm	LSCG & GDC	10–20 μm	Na	1 Ω cm^2	0.3 W cm^{-2}	723 K	25 ml min^{-1} 3% H_2O	1.8 mm O.d
Suzuki et al. [124]	ASC	Effect of anode microstructure on the performance of micro-tubular SOFCs	GDC	10	NiO–Gd doped ceria (GDC)	130 μm	5 μm & 0.2 μm	(LSCF)-GDC	10–20 μm	Na	0.1 Ω cm^2	0.6 W cm^{-2}	823 K	40% H_2 with 3% H_2O in N_2	0.8 and 1.6 mm in
Suzuki et al. [80]	ASC	Shrinkage behaviour and the microstructure of electrolyte/anode as a function of sintering temperature	GDC	Na	NiO	Na	Na	LSCF	Na	Na	Na	1.3 W cm^{-2}	873 K	ml min^{-1} + nitrogen 10 ml min^{-1}.	0.8 mm
Soderberg et al. [93]*	ASC	Comparison of MT-SOFC and planar SOFC performance.	YSZ	10	Ni–YSZ	220 μm	Na	LSM/LSM–YSZ	30–50 μm	0.4–0.2 μm LSM/YSZ	0.9 Ω cm^2	1073 * 0.212 W cm^{-2}	1073 K * 823 K	5 ml min – 30% H_2 in He^1	3 mm Od.
Sarkar et al. [125]		*Description of manufacture of MT-SOFC and testing.								0.8–0.4 μm LSM				*30 ml min^{-1} 3% H_2O in H_2	
Yamaguchi et al. [118]	CSC	Cathode-supported SOFC with new type of cathode material and combination.	GDC	Ca. 20–30	Ni/GDC	10 μm	GDC 0.3 Ni 1 μm	LSM, GDC, ScSZ	400 μm	LSM 3 μm and GDC 1 μm.	1.7 Ω cm^2	0.453 mW cm^{-2}	1023 K	30%H_2/N_2 (3% H_2O) *Pure Oxygen on cathode	Outer 1.6 mm and inner 0.8 mm
Dikwal et al. [126]	ASC	Thermal cycling	YSZ	15	Ni–YSZ	200 μm	Na	50% (YSZ) and 50% (LSM).	50 μm	Na	Na	0.6 W cm^{-2}	1073 K	20 ml min^{-1} H_2	Na
Lee et al. [59]	ASC	700w stack development	YSZ	5	Ni/YSZ	Na	Na	LSM/LSCF	Na	Na	Na	0.54 W cm^{-1}	1073 K	15 l min^{-1} (36 cells)	10 mm

Suzuki et al. [109]	ASC	Fabrication of micro-tubular solid oxide fuel cells with a single-grain-thick yttria-stabilised zirconia electrolyte	YSZ	1	Ni/YSZ	Na	Na	(LSCF/GDC)	Na	Na	0.03 Ω cm^2	0.39 W cm^{-2}	873 K	40 ml min^{-1} H_2 3% H_2	1.7 mm
Sarkar et al. [127,128]	ASC	EPD to fabricate laminated ceramics one end closed fuel manifold	YSZ	10	NiO	250 μm	Na	YSZ/LSM FL & LSM WL	10 μm & 20–30 μm	Na	0.4 Ω cm^2	0.25 W cm^{-2}	1073 K	30% H_2 + He mixture or pure hydrogen fuel	22 mm
Buchinger et al. [129,130]	ESC	Wood gas and methane in MT-SOFCs	YSZ	200	Nickel–YSZ 5% CeO_2	Na	Na	LSCM	Na	Na	1–2 Ω cm^2	200 mw cm^2	1173 K	Synthetic wood gas & CH_4/H_2	2.7 mm
Zhang et al. [101]	ASC	Hollow fibre cell with red-ox stable cathode	YSZ	10	NiO/YSZ	Ca. 225–275 μm	Na	LSCM–SDC–YSZ	25 μm	Na	0.4 Ω cm^2	0.4 W cm^{-2}	1073 K	40 ml min^{-1} H_2 with 3% H_2O	1.5 mm
BMVIT [131]	ASC	Report of the BMVIT project of Austria	YSZ	5	NiO/YSZ	300 μm	Na	LSM	50 μm	Na	Na	0.36W cm^{-2}	1073 K	Ca. 100 ml min^{-1} H_2 3% H_2O	2.7 mm
Zhao et al. [113]	ASC	Proton conduction cell	BZCYYb	25	NiO–BZCYYb	200 μm	Na	LSCF, BZCYYb	50 μm	Na	0.35 Ω cm^2	0.26 W cm^{-2}	873 K	(3 vol% H_2O in H_2) with a flow rate of 30 mL min^{-1}	<2 mm
Mirahmadi and Valefi [132]	ASC	Temperature distribution in a IR-MT-SOFC	8 YSZ	50	Ni–YSZ	2 mm	Na	La_{08} Sr_{02} MnO_3	25 μm	Na	Na	0.49 W cm^{-2}	1073 K	?H_2?	7 mm
Kawakami et al. [133]	ASC	Na	LDC ~ O (G ~ ZO ~)-LS	Na	NiO–YSZ & NiO–GDC10	Na	Na	LSCF	Na	Na	Na	0.85, 0.7, 0.25 W cm^{-2} at 700, 600, 500 °C	Na	50% N_2 50% H_2 1.2 l min^{-1}	5 mm

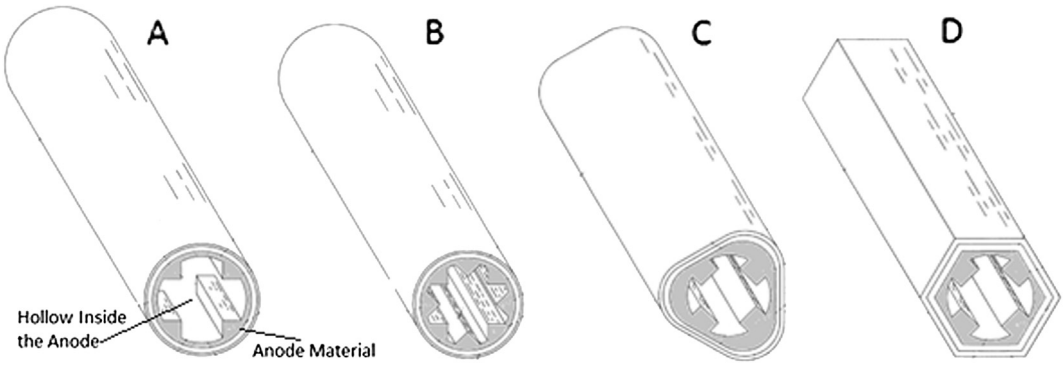

Fig. 1. A selection of images from the US patent of Finnerty and Coimbra [58]. Where A and B illustrate *conventional* shaped MT-SOFCs with non-conventional hollow anode interiors and C and D illustrate *non-conventional* MT-SOFCs with non-conventional hollow anode interiors.

electronic and ionic conductor. More of the ceramic ionic conductor allows a better thermal expansion match with other cell components, while less of the metallic electron conductor increases the anode's electrical resistance.

Supplementary to Ni and Cu which are the most prevalent catalyst and electron conductor materials, the addition of other metals such as (Pt, Rh, or Pd) are also being investigated as anode materials [76]. However, as yet, none of these three materials have been reported in MT-SOFC anodes. The high chemical stability in the electrochemical oxidising environment and catalytic activity when oxidising hydrogen or hydrocarbons makes these materials suitable anode constituents. State of the art SOFC anode material advances, up to 2007, have been reviewed by Sun and Stimming [77]. The authors discuss the material aspects, kinetics and cost-effective anode fabrication regarding the larger SOFC types, which is also relevant for MT-SOFC systems. Cimenti and Hill [78] have provided the essential anode characteristics, should the base fuel be a vaporised liquid.

Yamaguchi and Sammes [79] have recently reported that when the cathode is used as the mechanical support, in MT-SOFC design, the anode thickness becomes very important. The MT-SOFCs reported, with anode film thicknesses of 8, 30 and 50 μm, generated a maximum power density of 36, 49 and 126 mW cm^{-2}, respectively. The cell with a 50 μm thick anode layer showed about 10 times higher exchange current density than any of other cells. This would indicate that the anode's thickness affected the cathode-supported MT-SOFC performance.

As can be seen in Table 1 the vast majority of MT-SOFC groups tend to use Ni/YSZ or Ni/GDC based anodes. YSZ was originally used since it provides electrical isolation properties at high temperatures. GDC has been used in order to reduce the anode overpotential. However, GDC is not suitable at high temperatures as it conducts electrons.

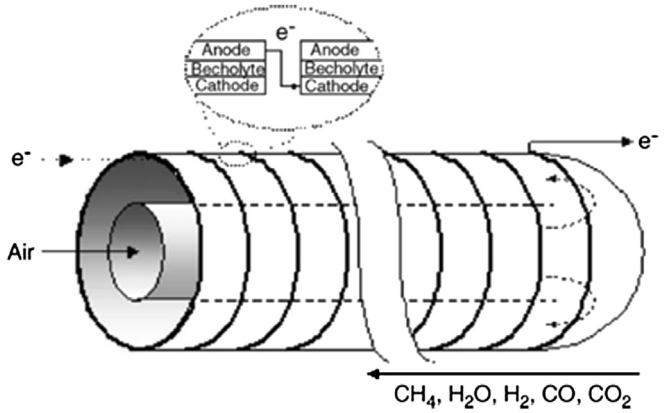

Fig. 2. The cascaded design of Nether [62] note that the single tube comprises of a number of cells.

For a very high performing MT-SOFC 1.2 W cm^{-2} at 600 °C, using standard SOFC materials GDC/YSZ and an Ni based anode support, Suzuki et al. [80] discussed the MT-SOFC anode's porosity and pore diameter distribution as a function of sintering temperature. They also describe how the density of the electrolyte layer that was deposited on the support surface was greatly affected by the shrinkage of tubular support during the co-sintering process. Moreover, up to 1200 °C, it was reported that the total pore volume decreased as the sintering temperature increased without effecting the pore size distribution.

Navarro et al. [81] have investigated samarium-doped ceria (SDC) as the ion conductor in a MT-SOFC design. An advantage of using SDC over YSZ is that it is an electronic and ionic mixed conductor under reducing environments. Navarro et al. [81] state that this may allow an anode triple phase boundary length increase, which would improve the anode's performance. However, the SDC anode based MT-SOFC performance data was not provided. Such data will be very interesting once established. The good catalytic properties of SDC, for the oxidation of hydrocarbon fuels, are also an interesting feature, particularly regarding intermediate temperature operation with hydrocarbon fuels. Ni–SDC is does not catalyse carbon deposition and thus catalyst deactivation can be diminished.

Phase inversion as opposed to conventional extrusion is another method used in order to control the anode microstructure and this method is discussed in Section 4.3. Methods of producing MT-SOFCs including the anode are discussed in Section 4. In the future anodes that are durable and reliable in both SOFC and SOEC modes will become ever more interesting in order to exploit the dual mode operation capability of the technology. MT-SOEC/SOFC operation is discussed in Section 6.2.

The red-ox tolerability of the MT-SOFC anode is also important, should regeneration cycles using oxygen be required for other system components or indeed in order to withstand leek oxygen infiltration into the fuel. A general review of red-ox problems associated with SOFCs can be found in Sarantaridis and Atkinson [82]. Recently Monzon and Laguna-Bercero [83] have reported experimental results for red-ox cycled MT-SOFCs. In the event of fuel contamination a rapid shut-down may be possible in MT-SOFC systems. Rapid shut-down is not an option for larger SOFC systems. Monzon and Laguna-Bercero [83] studied red-ox cycling and found that MT-SOFCs that had a similar low tolerance for red-ox cycles with more or less the same damage mechanisms and results are reported for larger SOFCs, refer to Ref. [82].

The main problem with regard to state of the art reports dealing with red-ox tolerance is that they all deal with air as the oxidiser, e.g., Refs. [84–86]. Using oxygen and hydrogen would not be a wise testing methodology; considering the inherent dangers at high temperature. Anode oxidation with mixes of hydrocarbon fuels is much more relevant for commercial application and the field has not addressed this to any significant degree. In MT-SOFC systems using hydrocarbon fuels, oxidation will likely occur electrochemically, a result of high fuel utilisation, since under normal conditions either carbon deposition or anode re-oxidation will occur, as demonstrated in a ternary plot of Ref. [87]. The risk of anode re-oxidation as a result of oxygen reaching the anode with hydrocarbons will be considerably low as CPOX will eliminate this risk. A study that characterises MT-SOFC electrochemically induced red-ox cycles in hydrocarbon fuels would be very interesting.

Gemmen and Johnson [88] show, a rare plot, highlighting how even relatively small changes of fuel utilisation for a 97% H_2 and 3% H_2O mix had a significant impact over significant periods of time. They showed that for 80% fuel utilisation no observable degradation occurred while for 85% fuel utilisation significant degradation per day occurred. This degradation was a result of some fuel starvation and subsequent anode oxidation at the higher fuel utilisation. The anode material is critical regarding hydrocarbon reforming and the reader is pointed to Section 5 in order to find out more about anode material selection.

Current collection from MT-SOFC anodes is not as simple in comparison to larger tubular and planar SOFC designs. Since the hollow channel inside the MT-SOFC is so narrow and furthermore the insertion of instruments inside this hollow adds the risk of; poor contact, increased back pressure and increased manufacture cost, other methods of current collection are of interest. Suzuki et al. [89] showed by comparing single and double terminals for current collecting that the efficiency loss estimated from the double terminal model was about 2–4 fold lower than the efficiency loss obtained from the single terminal model. As a single terminal current collection method is more preferable, as outline above, Suzuki et al. [90] tried to increase the anode conductivity by producing a Ni–Fe anode support. It was shown that similar porosity to Ni designs with 2–3 μm pore size was achievable for various sintering temperatures. However, some diffusion related losses cause a high polarisation loss, which hindered the cell performance after reduction. Microstructure optimisation was recommended in order to improve the circumstance. De la Torre and Sglavo [91] have reported the successful implementation of metal wires into the MT-SOFC anode when a dip-coating method was used. This is a very novel approach that seems to have worked quite will, but the wires' effect on the MT-SOFC's long term mechanical stability, implications for red-ox tolerance and effect on concentration losses all need to be assessed.

3.2. The cathode

Oxide ceramics that are electronically conductive and have a good electro-catalytic activity are important SOFC cathode materials. Oxides are preferred because the cathode must be chemically stable in a calescent reducing environment. The most prominent material is strontium-doped lanthanum manganite (LSM, $La_{1-x}Sr_xMnO_3$). LSM is known to have a relatively high electronic conductivity ($\sigma_e > 10$ S cm^{-1} at 700 °C) [8] and it has good electro-catalytic activity, which is essential when oxygen should be reduced. The porous cathode can consist of LSM only, or a LSM and the electrolyte material composite in order to provide an improved three phase boundary coverage. As seen in Table 1 the majority of MT-SOFC groups tend to use LSM, LSCF or combinations, which also include GDC in order to aid thermal expansion coefficients. It has been reported that the cathode conductivity should have a lower limit of 200 S cm^{-1} [92].

With MT-SOFCs Soderberg et al. [93] compared the performance of a cathode that was brush coated onto a Ni/YSZ support with a standard planar cell. The tests showed that the brush-painted LSM–YSZ properties, evaluated using both ElectroChemical Impedance Spectroscopy (EIS) and Cyclic Voltammetry (CV), were similar in both the planar and micro-tubular test samples. A similar polarisation resistance value was obtained in both cases, showing that the impedance response of the LSM–YSZ on the thin YSZ electrolyte layer in the micro-tubular configuration was not being influenced by the characteristics of the Ni–YSZ counter electrode. The authors have discussed increasing LSM cathode performance by increasing the sintering temperature from 1100 K to 1150 K. It is known that increasing the sintering temperature changes the cathode's particle size, porosity, TPB length, and the cathode/electrolyte interface chemistry. Furthermore, their results indicated that the higher cathode sintering temperature improved the bonding between the electrolyte layer and the cathode, as well as the particle/particle contact within the cathode layer itself.

A matrix design cathode as seen in Fig. 3 has been developed with much success by a prominent research group in Japan [6,94,95]. These cathode matrix designs are unique to the MT-SOFC, although for planner designs anode and cathode matrix designs are of interest. In this design the cathode has three main functions; firstly to act as the current collector, secondly to be a guide where the electrolyte/anode component fits in and thirdly they define the flow paths for the air. Funahashi et al. [96] used a 20 μm particle size LSCF cathode in order to allow sensible resistance to the air inflow. The sintering temperature was also found to play a key role in the porosity and thus matrix air flow resistance. Changing the sintering temperature from 1300 °C to 1500 °C without a pore former was found to reduce the gas penetration coefficient. Mori et al. [92] also used a 20 μm particle sized cathode and achieved a 75% porosity in their cathode matrix.

In this study [92], highly porous $La_{0.6}Sr_{0.4}Co_{0.2}Fe_{0.8}O$ current collectors were homogeneously infiltrated by Ag nano-particles via the citric acid method in order to increase the matrix electrical conductivity. Although the Ag particles in the collectors were isolated and did not make contact with each other, an increase in thermal expansion coefficient and the electrical conductivity was

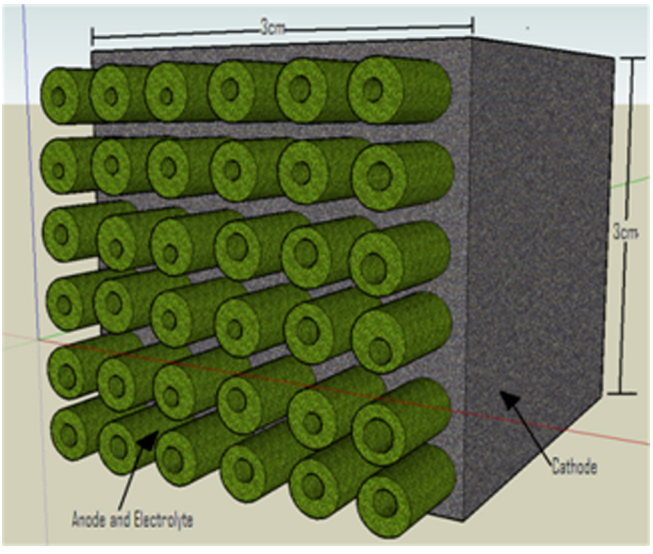

Fig. 3. An illustration showing the cathode matrix design of a prominent research group in Japan [6,94,95]. (Original figure in Ref. [46]).

observed. Infiltration by Ag increased the conductivity 3 fold and thermal expansion coefficient by 8% in comparison to the standard LSFC matrix. Oxygen vacancies and the increase in conductivity were related to the increased covalence of the Co, Fe—O bond. The dense LSCF sample had conductivities of 295 and 305 S cm^{-1} at 500 and 650 °C, respectively. The conductivity of LSCF with a porosity of 75% was 87 S cm^{-1} at both 500 and 650 °C. Interestingly, following treatment with the Ag baths 7 and 10 mol L respectively: conductivities of 170 and 220 S cm^{-1} at 550 °C were achieved. These results were explained by the well-dispersed, highly conductive Ag particles reducing the mean-free path of electrons, which to some degree, makes electron migration easier through the pore wall surface of LSCF via the active sites. The group reported problems with the matrix stability during the stack fabrication and other reports have indicated the instability of silver, especially at high temperatures [64,97–99].

Since these matrixes form a "foam structure" around the MT-SOFCs, heat removal is expected to be a consideration. Funahashi et al. [100] reported that the temperature distribution within a MT-SOFC bundle, encapsulated within mixed ionic conductor matrices with MgO, was more moderate when compared with the temperature distribution within LSCF matrices. This simulation finding was attributed to MgO's high thermal conductivity. The MgO based cathode had 450 ml min^{-1} air feed at 240 °C and 20% air utilisation. The bundle temperature distribution was predicted ranging from inlet 521 °C to outlet 555 °C. In comparison, they reported that a LSCF matrices' bundle temperature distribution ranged from 445 °C inlet to 566 °C at the outlet. In this case the inlet air flow rate was 247 ml min^{-1} at 265 °C and the stack performed with 20% oxidant utilisation [95]. Both these studies were simulation-based without a direct experimental validation or numerical solution analysis.

Zhang et al. [101] showed a hollow fibre single MT-SOFC with an outer diameter of 1.3 mm that produced OCVs close to the theoretical value and high peak power densities of 513, 408 and 278 mW cm^{-2} at 850, 800 and 750 °C, respectively. They attribute the high performance to the thin electrolyte and proper cathode having a low interfacial polarisation resistance. This work indicates that the red-ox stable LSCM—SDC—YSZ is a promising cathode material composite for the next generation YSZ-based HF-MT-SOFCs.

3.3. The electrolyte

The electrolyte is an extremely important SOFC component. The electrolyte must conduct oxygen ions and resist electron conduction while simultaneously being impervious to the fuel and oxidant species. The traditional material for both larger SOFCs and MT-SOFCs has been yttria-stabilised zirconia [102] (YSZ, $Y_{2x}Zr_{1-2x}O_{2-x}$, x = dopant concentration in mol-% Y_2O_3 in ZrO_2). This material was first tested by Baur and Price in 1937 [50] since it facilitates high-temperature superior ion conduction and electrical insulation, YSZ is still the most extensively used SOFC electrolyte material. Within the foreseeable future, no new electrolyte materials seem likely to replace the state of the art materials. Stabilised zirconia and ceria appear to be the best electrolytes presently available [103]. Zirconia's key advantage is that it is very stable under both oxidising and reducing environments; this is a unique material property. Doping, exchanges the Zr_{IV} cations of the ZrO_2 host lattice with Y_{III} cations. This leads to both, oxygen vacancies formation affording ionic conductivity and ZrO_2 cubic phase stabilisation. YSZ has a high conductivity for O^{2-}-ions but only at high temperatures ($\sigma_i \sim 0.1$ S cm^{-1} at 1000 °C, ~0.01 S cm^{-1} at 700 °C) [49]. Other dopant atoms (Sc, Ca, Mg, Nd, Sm, Yb) are also being trialled [53].

As can be seen in Table 1 the vast amount of MT-SOFC groups has made studies with YSZ or GDC electrolytes. 10 μm seems to be a target thickness but there are some reports under this size and many above. Although several compositions give better conductivities than YSZ, they are more expensive, not easily processed and profusely prone to chemical attack [104]. Bismuth oxide provides the highest ion conductivity, while cerium gadolinium oxide (CGO) and lanthanum strontium gallium magnesium oxide (LSGM) give significant benefits below 600 °C [105]. An additional ceria-based electrolyte problem is its electronic conductivity under the reducing atmosphere, which becomes noticeable above 600 °C. This results in electrode and counter electrode short-circuiting condition [106]. Of the known oxide-ion conductors, high-temperature δ-Bi_2O_3 has the highest conductivity, >1 S cm^{-1} at 800 °C, but it is stable only between 730 °C and 804 °C (its melting point).

Very recently Ahn et al. [107] have shown a fabrication technique applied to a dual-layer electrolyte. GDC single-layer electrolyte-based SOFCs were prepared from four different fabrication methods and exhibited maximum power densities ranging from 0.338 W cm^{-2} to 1.03 W cm^{-2} at 650 °C. At each fabrication stage, an Erbium-stabilised Bismuth Oxide (ESB) layer was applied to form a bi-layer electrolyte. A maximum power density of 1.95 W cm^{-2} and 0.079 Ω cm^2 total cell ASR was achieved at 650 °C for a bi-layer cell, combined with their recently developed BRO7-ESB ($Bi_2Ru_2O_7$ — Erbium-Stabilised Bismuth oxide) composite cathode. The group demonstrated that the bi-layer electrolyte combined with the special cathode reduced the total area specific resistance (ASR) from 0.126 Ω cm^2 for a single-layer GDC electrolyte to 0.079 Ω cm^2 for the BRO7—ESB combination. This increased the cell's maximum power density from 1.03 W cm^{-2} to 1.95 W cm^{-2}

Lower temperature SOFC operation, from 1000 °C to 750 °C, would allow common material metal interconnects and this has encouraged scandia stabiliser in order to replace or augment the yttria normally used in YSZ electrolytes [104]. However, even with such modifications to the electrolyte mechanical properties and prolonged high temperature and red-ox exposure degradation is still an overwhelming concern. Start-up and shut-down temperature changes can cause large cell component movement gradients, which then causes the electrolyte to crack as a result of low strength [108]. Thus finding electrolyte materials having lower thermal expansion coefficients is advantageous. Kendall has suggested developing silica based electrolytes [104], which would have a lower coefficient of thermal expansion. This would imply that smaller component movement would occur in the SOFC during start-up. Recently Suzuki et al. [109] published their study on the fabrication process and electrochemical MT-SOFCs performance analysis of a single-grain-thick YSZ layer electrolyte upon a Ni/YSZ anode. They found that a uniform electrolyte slurry coating and controlled supported anode tube shrinkage, achieved by changing the sintering temperature, led to a dense, crack-free, single-grain-thick electrolyte. Their MT-SOFC produced a power density of 0.2 and 0.39 W cm^{-2} at operating temperatures of 550 and 600 °C, respectively. However, the robustness of such a design during long term operation is not proven and would be a concern.

Current electrolyte field research tends to focus on reducing the operating temperatures below 600 °C. Gadolinium-doped ceria (GDC) is generally regarded as the most promising candidate. It has a high ionic productivity and also a high electrical resistance around the 600 °C temperature range. As seen in Table 1 many MT-SOFC groups have reported using this material. Its ionic conductivity ($\sigma_i \sim 0.05$ S cm^{-2} at 700 °C) is approximately five times higher than YSZ [110]. However, at low oxygen partial pressures and at higher temperatures ceria is partially reduced and the material becomes an electronic conductor, which of course is

counterproductive. Zirconia- and ceria-based electrolytes have a cubic, fluorite-type crystal structure. Having this structure affords the large oxygen ions a high mobility. Oxides with a perovskite structure have also been used in order to facilitate high ion mobility. For example strontium- and magnesium-doped lanthanum gallate (LSGM, $(La_{1-x}Sr_x)(Ga_{1-y}Mg_y)O_{3-\delta}$) [3].

Recently, proton-conducting materials (e.g., barium cerate, BaCeO3) have been studied as electrolytes, opening up a completely new solid oxide fuel cell type [111]. Proton-conducting ceramics have been reported to have large conductivities and are becoming comparable with state of the art ion conducting ceramics with extra potential for high proton conductivity at low operating temperature. The advances made recently in improving the "sinterability" of the powders, bringing the sintering temperature at values similar to those needed for yttria-stabilised zirconia (YSZ), and therefore allowing the processing at temperatures compatible with mass production, powder-based, low-cost fabrication technologies, show potential for the development of a next generation of anode-supported MT-SOFCs based on proton-conducting electrolytes, operating at 600 °C with hydrogen or even hydrocarbon and alcohol fuel [112]. However, despite the recent progresses in electrode development, the practical use of these electrolytes is yet to be realised, owing mainly to the very large cathode overpotentials observed at low SOFC operating temperature. The reader is pointed to the review by Fabbri et al. [112] for an account of proton-conducting SOFCs.

There are some notable accounts of proton-conducting MT-SOFCs. For example, Zhao et al. [113] have published an account for a 1.6 mm diameter MT-SOFC composed of NiO–BZCYYb, BZCYYb and LSCF–BZCYYb (BZCYYb is $BaZr_{0.1}Ce_{0.7}Y_{0.1}Yb_{0.1}O_{3-\delta}$) as anode, electrolyte and cathode, respectively. Maximum power densities of 0.08, 0.15, and 0.26 W cm^{-2} with the OCV values of 1.05, 1.03 and 1.01 V were reported at 500, 550 and 600 °C, respectively. Chen et al. [114] used a dip-coating method and fabricated 1.6 mm diameter MT-SOFCs based on BZCYYb electrolyte. The Ohmic resistance was 0.1 and 0.3 Ω cm^2 at 750 and 600 °C, respectively. The peak power density was reported as 1.13 and 0.53 W cm^{-2} at 750 and 600 °C, respectively.

Finnerty and Coimbra [115] have described a novel MT-SOFC and production process for a cell with a "cermet" electrolyte. Under operating conditions a dense electrolyte and metal oxide sub-layer would exist on the electrolyte oxidised side (cathode side). While the other side of the electrolyte (reducing side) would be made of a porous sub-layer containing transition metal. The tailoring of the amounts of metal present in the anode and the cermet electrolyte could allow for greater power output and enhanced electrochemical performance, while maintaining the structural integrity and reliability of the SOFC. There is no other published data showing that such a concept would function. Nonetheless, the novel electrolyte architecture is worth a mention.

3.4. Metal supported MT-SOFC

Metal supported cells could be considered the third generation of SOFCs. They should be considered the next evolution after anode and cathode-supported designs. To date, in the MT-SOFC field, very few publications relating to metal supported MT-SOFCs are available in the literature. A comprehensive and interesting metal supported SOFC review has been written by Tucker [116]. In this paper metal supported SOFC's benefits discussed include; increased mechanical ruggedness, red-ox tolerance and rapid thermal cycling. It is often stated in metal supported SOFC papers that the mechanical ruggedness is a very useful attribute should SOFCs be used in automotive applications where shocks and vibrations will occur. However, there is no literature or test results available explicitly stating exactly how much more rugged a metal supported cell would be. In fact, protection of the electrolyte should be considered most important, since this is the component that should not receive any unnecessary stress. Indeed, removing anode or cathode material and replacing it with a metal support may not provide any extra protection to the electrolyte in such applications. Proof that metal supported SOFCs help to protect the electrolyte under vibrations or shocks is required. Furthermore, metal supported SOFCs may even add additional stresses to the electrolyte since their thermal expansion is significantly greater.

A metal support may allow a geometry flexibility that ceramic manufacturing process cannot achieve easily and inexpensively. This coupled with the reduced requirement for more expensive anode and cathode material and the potential reduction of SOFC ohmic resistance is more likely why metal supported cells are of importance. Tucker [116] described how a metal support may relieve and induce desirable stresses within the MT-SOFC, most notably when operating in cold conditions.

4. Methods of producing MT-SOFCs

MT-SOFC production is certainly not a trivial matter. Should MT-SOFCs be mass produced, the cost per MT-SOFC and their reliability becomes key considerations. While the MT-SOFC is still very much in the R&D phase, plenty of literature is available discussing and describing SOFC manufacture. A good summary, is published in 2007 in the DOE/NETL report [56], in which different processing methods used to produce large SOFCs are detailed.

A brief summary of MT-SOFC production methods and reports thereof has been provided in the thesis of Garcia [134]. For MT-SOFCs the most often reported methods for manufacture include extrusion of the substrate and co-extrusion of different layers [135], dip coating in order to produce substrates and layers [136–138], EPD to produce layers on substrates [125], spray coating to produce layers [139] and brush painting to produce layers [93]. These methods and more that are used in order to construct larger SOFCs are summarised in Table 2. The following sections will provide more detailed information regarding MT-SOFC manufacture and manufacturing techniques.

4.1. Extrusion and injection moulding

Conventionally, the MT-SOFC requires one of the cell components, which can be the anode, electrolyte or cathode to function as a substrate for the deposition of the remaining cell layers. Furthermore, this substrate subsequently functions as the MT-SOFC mechanical support after cell manufacture. As seen in the literature reports, to date, extrusion is often favoured for substrate production because of low cost and well developed technologies and techniques. The problems associated with extrusion include maintaining straightness during the firing process, obtaining thin walls without defects and preventing sagging of the circular

Table 2
Common SOFC processing methods for each material preparation step outlined in the DOE/NETL report [56].

Raw material production	Forming	Conditioning
Powder production	Extrusion	Drying
Powder preparation	Tape casting	Bisquering
Size reduction/milling	Dip coating	Sintering
	Flame/plasma	
	EVD	
	CVD	
	Sputtering	
	Calendaring	

cross-section to a more oval shape. The tubes can also warp and twist during binder removal and air/binder bubbles formed during the process are very undesirable.

Currently the main groups publishing MT-SOFCs literature employ conventional extrusion techniques in order to produce substrates that are coated with electrodes. Reports for electrolyte supported cells can be found in Refs. [129,130,140] or anode or cathode supported in Refs. [118,128,141,142]. Up to recently, a project consortium including mainly Austrian and German partners [131] worked together, aiming to develop MT-SOFC mass production techniques. Their research focused not only targeting MT-SOFC production but also targeted developing cost-effective manufacturing processes. In a final project report [131] lots of information can be found regarding their attempts to simultaneously co-extrude NiO and NiO–YSZ anode layers. The consortium developed a special tool that allowed nickel tube production using a preliminary injection moulding procedure, which was subsequently "over-moulded" with a NiO–YSZ anode layer.

A major Japanese group in the MT-SOFC field, refer to Funahashi et al. [96], also mention that their MT-SOFC tubes were extruded from a metal mould using a piston cylinder type extruder. The Japanese company TOTO and partners [133] have extruded anode substrates and then applied a slurry coating for the electrolyte and cathode [33]. However, no information has been provided regarding their extrusion apparatus or technique. Jardiel et al. [143] have used a polymer-based and a thermoplastic powder extrusion moulding system with high solid loading to obtain 200 μm thick YSZ tubes.

Regarding the extrusion optimisation of substrates little information is publicised for obvious reasons. But for example, Du et al. [144] produced thin, dense, smooth finished and straight YSZ tubes that could be extruded using either water-based or organic additives. They found in order to manufacture high quality tubes that using water-based additive system accorded a higher success rate, when compared to the organic based additive. The authors also explained that the particle size distribution is an important consideration so that good pastes required for well shaped tube manufacture are yielded. Their results after sintering showed that the substrate microstructure had a sufficiently sintered MT-SOFC material with adequate micro-pores for fuel distribution.

Important to note is that after extrusion, the layers of the remaining cell components may be deposited using techniques such as dip coating [136–138], chemical vapour deposition (CVD), electro-phoretic deposition (EPD), plasma spraying or a pneumatic spray technique, followed by various sintering procedures. These manufacturing methods are time consuming and often very expensive. The BMVIT project report [131] describes how the electrolyte and cathode layers were deposited onto an extruded substrate by using a spraying technique. The quality assurance issues that the consortium found when spray coating the electrolyte layer are also discussed. Furthermore, an electrolyte layer deposited by using electrophoresis deposition technique is discussed. MT-SOFC production methods can also be found in the following; in Song et al. [145] a preparation of materials for extrusion, in Lee et al. [146] a method of manufacturing micro-channel tubular solid oxide fuel cell using multi-pass extrusion process, in Devoe et al. [147] a unique production method, whereby laminate thin-wall ceramic tubes are constructed is described.

Co-extrusion of all the MT-SOFC layers would be a very worthwhile technique if it could be successfully achieved. To this aim, Powell and Blackburn [135] showed that anode and electrolyte paste rheologies can be unified allowing simultaneous extrusion. In their study they showed that the experiment quantity, a perquisite in order to derive a good paste rheology, is reduced when acquired packing behaviour knowledge is obtained. This allows an intermediate composition formulation calculation. They also described the paste mixing consideration's importance regarding the rheology residuum.

4.2. Other approaches for MT-SOFC manufacture

While extrusion has been favoured by many groups in order to produce MT-SOFCs this method is not the only possibility and other methods that may afford cheaper manufacture, more reliability and/or increased simultaneous production are of interest. In fact, a method that could produce a bundle of MT-SOFCs complete with a ceramic or metallic manifold would be extremely useful. However, considering the difficulty involved in producing single cells, this may be a far-fetched concept.

Dip coating, although it initially seems like a very crude method in order to produce MT-SOFC substrates has been shown to be quite sufficient. This coating process can be easily automated in comparison to the conventional extrusion process and would have a lower machinery investment cost. For example, Kikuta et al. [137] have developed a multi-dip-coating method in order to manufacture MT-SOFC substrates. The produced MT-SOFCs showed good linearity and a maximum power density of 0.14 W cm^{-2} at 550 °C. In order to make the MT-SOFCs, initially steel wire was coated with a polystyrene polymer toluene solution, thus preventing NiO–GDC to steel adhesion. The substrates were dipped firstly into an anode NiO–GDC bath twice followed by the GDC electrolyte and LSM–GDC cathode coats. Ramping the MT-SOFC temperature until 500 °C at 2 °C min^{-1} caused binder scorching.

They found that by adjusting the ceramic and binder slurry contents and coating times, controlling the electrode and the electrolyte layer thickness was possible. Manufacturing a MT-SOFC by dipping is quite an achievement in itself, especially considering the 100 μm anode substrate layer wall thickness. Kikuta et al. [137] MT-SOFCs performed quite reasonably, especially considering for both, the cathode and the anode, a pore former was neglected and the electrolyte thickness was 33 μm. Also, the LSM cathode would not be considered optimal and cell performance may be improved by selecting an alternative cathode material. The mechanical reliability of the anode substrate may also require some scrutiny.

An attempt to fabricate flattened ribbed cells via the dipping process was also attempted by this group [137]. However, the stack performance was not tested because a suitable manifold method was not available. Regardless, this multi cell bundle manufacture simplicity is impressive and much less cumbersome than other manufacturing methods. Applying the dip-coating method in order to produce metal supported micro-tubular SOFCs seems like a plausible evolution. In this case, nickel meshes wound around the inner steel wires could be used as the MT-SOFC support. In fact, a patent by Sarkar et al. [148] states how this can be achieved when porous metallic supports are used.

Tan et al. [149] have explained that among the existing technologies used in order to prepare ceramic films, the colloid methods such as the sol–gel and the dip-coating, in which the ceramic electrolyte film is firstly formed from a solution and then sintered at a high temperature, can produce thin electrolyte films with low cost, but the obtained films are easily cracked, while the deposition methods such as the chemical vapour deposition (CVD), electrochemical vapour deposition (EVD), sputtering, vacuum plasma spraying and the pulsed laser deposition (PLD) always require expensive equipment and consequentially a high production cost. The preparation of electrolyte films for MT-SOFCs using the conventional techniques such as the sol–gel and the CVD-EVD requires more trenchant operating conditions, leading to a noticeable increase in the production cost of micro-tubular fuel cells.

Very recently, Navarro et al. [81] successfully produced MT-SOFC substrates using a cost-effective gel-casting technique.

The rheological parameters of the ceramic particle suspensions, directly influencing the casting and production, were investigated. The MT-SOFC tubes were formed by using a simple technique based upon a syringe, punch and their own die. An SDC electrolyte was then deposited on the anode using a colloidal spray technique. An LSC cathode was subsequently sprayed onto the cell. The manufacturing techniques were proven to function, but to date, no electrical characterisation of the MT-SOFC has been published.

Alberta Research Council [93] used a very interesting method to produce their 2–3 mm diameter MT-SOFCs. The anode layer, which was also the support, was deposited onto a carbon rod using EPD. The first layer deposited was the Ni–YSZ layer and then a YSZ electrolyte was subsequently deposited. The MT-SOFC was heated until the carbon rod was burnt away. The anode and electrolyte were also sintered in this step. The cathode was then brush coated onto the YSZ electrolyte. Sarkar et al. [125] discuss in detail the critical issues and potential strategies that avoid EPD problems and produce good layers. The EPD process versatility allows a wide composite microstructure spectrum fabrication. However, the cost required in order to manufacture cells this way may be a deterrent. Especially, brush coating seems impractical for mass production.

4.3. Hollow fibre MT-SOFC's

Very recently hollow fibre MT-SOFC's have been achieved by using phase inversion and sintering techniques. NiO/YSZ hollow fibres can be fabricated, for example Ref. [150], via a combined phase inversion and sintering technique. Whereby, polyethersulfone (PESf) is employed as the polymeric binder, *N*-methyl-2-pyrrolidone (NMP) as the solvent and polyvinylpyrrolidone (PVP) as the additive. After a reduction with hydrogen at 750 °C for 5 h, the porous Ni/YSZ hollow fibres with an asymmetric structure comprising of a microporous layer integrated with a finger-like porous layer can be realised. A tubular substrate produced by this method can be used as the anode support of MT-SOFCs.

Compared to conventional ceramic extrusion methods discussed previously, the hollow fibre method allows tube inner structure control. Most importantly, the pore size can be decreased gradually from the outside surfaces to the fibre's centre. This means, good microstructures providing improved gas diffusion and a high performance active zone can be created aiding optimal electrolyte deposition. It may also be possible that hollow fibre producing techniques can produce cells with dimensions and lengths not achievable when using conventional extrusion [151]. Anode polarisation loss reduction in comparison to extruded MT-SOFCs may also be achievable [138]. A combined co-extrusion and co-sintering technique has the potential to produce electrode/electrolyte dual-layer hollow fibres in a single step.

Regarding a summary of hollow fibre MT-SOFCs the following accounts are relevant. A stack design and method for producing MT-SOFCs using the phase inversion method with a novel manifold design is discussed in Ref. [152]. Chen et al. [138] performed a dip coating and phase inversion, Othman et al. [153] describe a method whereby a triple orifice spinneret was used in order to produce the MT-SOFCs. Zhang et al. [101] also used a spinneret mechanism. Grande et al. [154] described an electro-less plating method. Electro-less plating consists of Ni^{2+} ion reduction to metallic Ni by a reducing agent (sodium hypophosphite).

Table 3 below shows some performance data regarding these hollow fibre type MT-SOFCs. As can be seen the powers produced by these types of cells are still some way off those achieved cells manufactured by other methods as seen in Table 1. Also worth noting is that the dimensions of these types of cells are tiny, generally between 1 mm and 2 mm in diameter.

4.4. Metal supported MT-SOFC and their manufacture

As stated previously there are no significant reports relating metal supported MT-SOFCs. Their manufacture and design is state of the art and since they are not yet reportable for MT-SOFCs they are outside the scope of this paper. However, as a brief prognosis, metal foams seem like ideal candidates for MT-SOFC supports that could indeed provide all the benefits listed by Tucker [116]. Since MT-SOFCs inherently have a high thermal shock tolerance and are already considered ideally suited for APU and possible automotive applications, a metal supported MT-SOFC with a metal foam or metal mesh may be a highly desirable, inexpensive and easy to manufacture MT-SOFC type. However, not much literature exists regarding such a MT-SOFC and avoidance of any extra stress to the MT-SOFC electrolyte needs to be minimised and thermal any expansion mismatch carefully considered. For example, Sarkar and Hongsang [68] have discussed a stack design incorporating metal foam. Other metal supported SOFCs descriptions include bi-tubular support design discussed in Ref. [156] and a combined porous and solid supported SOFC [157].

Rementeria et al. [158] have disclosed a SOFC, possibly micro-tubular, adapted and connected to a gas fuel supplying system. This system has an inner tubular electrode, which is deposited on a metal support upon which, the first electrode is deposited. At the threaded first end, the tubular SOFC is tightly fixed to an inlet manifold. This is an example where a metal support can also be used to simplify the MT-SOFC-gas manifold.

Villarreal et al. [159] have outlined the manufacture of powder metal tubes, which were prepared by scalable cost competitive routes. It is not clear if their SOFCs could be scaled down to the MT-SOFC scale. A ceramic barrier layer was deposited to prevent Cr, Fe and Ni inter-diffusion between the support and anode layer. A thin electrolyte was then deposited by dip coating and then co-fired in an oxidising atmosphere at 1350 °C. The composite cathode was subsequently dip coated and fired in situ prior to electrochemical characterisation. Tubes of 10 cm length with an active an area of 25 cm^2 were systematically achieved. The authors explained tremendous effort was devoted to prevent Cr–Fe–Ni inter-diffusion at the anode side of the cell. For that reason, several ceramic materials were developed and processed as protective barrier layers.

Smorygo et al. [15] studied metal foams of Ni, Fe–Cr steel and Ni–Al inter-metallic as candidate for catalyst supports, allowing intermediate temperature SOFC internal methane steam reforming. While this account is not specifically related to MT-SOFCs, for metal supported MT-SOFCs the information may well be relevant. All foam candidates showed good catalyst adhesion and stable catalyst performance was achieved in the Ni–Al foam support case. The Fe–Cr support reacted with active components, which caused fast catalyst deactivation. The support porosity was 75–95% porous and porosity did not remarkably affect the catalyst performance. Therefore, $(Pr_{0.3}Ce_{0.35}Zr_{0.35}O_2)$/NiO/8YSZ and $(La_{0.8}Pr_{0.2}Mn_{0.2}Cr_{0.8}O_3)$/NiO/8YSZ composite catalysts supported on Ni–Al open cell foams can be applied for IT-SOFC indirect internal steam reforming. Kurokawa et al. [160] have developed an effective water-based binder system for co-firing porous alloy supports with electrode/electrolyte structure for SOFCs.

4.5. Conclusions regarding MT-SOFC manufacture

As highlighted in this section there are many different manufacturing techniques being developed for MT-SOFC manufacture and it is still not clear which method or methods are the most cost effective, reliable and produce cells that deliver significant power in a durable and reliable way. With metal supported

Table 3
Reports of hollow fibre MT-SOFCs.

Report	°C = mW cm^{-2}	Fuel	Cell diameter (mm)	Ω cm^2 at °C
Zhang et al. [101]	750 °C = 278 mW cm^{-2} 800 °C = 408, 850 °C = 513	40 ml min^{-1} 3% H_2O	1.3	0.14, 0.29 and 0.59 Ω cm^2 at 850, 800 and 750 °C
Droushiotis et al. [155]	450 °C = 42 mW cm^{-2} 550 °C = 80 mW cm^{-2} 580 °C = 100 mW cm^{-2}	5 ml min^{-1} 100% H_2	1.4	2–6 Ω cm^2 at 450–580 °C
Grande et al. [154]	800 °C = 1–6 mW cm^{-2}	30 ml min^{-1} 95% Ar 5% H_2	1.6	NA
Chen et al. [138]	800 °C = 752 mW cm^{-2}	30 ml min^{-1} 3% H_2O	2	0.75 Ω cm^2 at 800 °C

cells expected soon to be state of the art SOFC technology, the progress of MT-SOFC manufacture is an extremely relevant and worthwhile field. An enclosed, not necessarily tubular, but to the same scale, SOFC based on the metal supported architecture could hypothetically be designed to have a geometry that favours important cell attributes and indeed increase a MT-SOFC's active are.

5. Internal reforming in MT-SOFCs and usage with hydrocarbon fuels and reformates

SOFCs offer potential advantages in terms of cost and efficiency over other fuel cell types. This is compounded by the necessary high SOFC operating temperature that facilitates running the SOFC using natural gas or other hydrocarbon fuels. Three different operating modes are possible when a SOFC is fuelled with hydrocarbon fuels. These modes are external reforming, internal reforming, and direct oxidation/direct utilisation. In the first two cases, the purpose is to completely convert the fuel into synthesis gas that is sub-sequentially electrochemically oxidised. These fuel reforming methods are explained in detail by Cimenti and Hill [78], where the authors notably point out the general lack of direct internal reforming studies. Highlighted by this review, is that those studies published tend to focus on methane as the fuel. Furthermore, studies considering direct partial oxidation application and auto-thermal reforming appear sparsely in the literature for MT-SOFCs.

5.1. Fuel cell degradation with hydrocarbon fuel: re-oxidation and carbon deposition

Problems associated with MT-SOFC internal reforming includes carbon formation on the anode, anode particle sintering, anode leaching and delamination and the intrinsic strong endothermic disposition, when steam reforming. This section will provide an account of state of the art MT-SOFC degradation and relevant SOFC degradation studies. This approach is required since very little literature deals with MT-SOFC performance degradation as a result of hydrocarbon fuel use.

Regarding re-oxidation, the work of Ettler et al. [84,161] is currently state of the art regarding SOFC single cells and stacks. The study is based upon a comprehensive study regarding planar SOFCs and the effect of red-ox cycles. It clearly shows that constraining the planar SOFCs in cassettes causes irreversible damage due to anode deformation. In Ref. [161] an attempt was made to use measurement data in order to develop a model/mathematical relation that predicts the damage caused as a function of several cell fuel features. A very important concept regarding the warping of planar SOFCs, which is a function of; temperature, partial pressure of oxidant in the fuel, fuel flow rate, anode substrate porosity, is the NiO/Ni boarder that develops between the oxidised anode and remaining reduced anode. This border is more clearly observed at higher temperatures. Oxidation of the anode begins at the regions close to the gas channel and it proceeds inwards; towards the electrolyte. The increased volume, attributed to the NiO, then causes the cell to warp, whereby the electrolyte and cathode are forced into compression along their lengths. As this oxidation grows into the anode and passes through the centre of the anode material, the expanding anode causes the cell to warp in the opposite direction causing the electrolyte and cathode to be in tension. Consequentially, this then leads to cracks in the electrolyte. Similar observations regarding the mechanical deformation of planar cells can be found in Stathis et al. [162].

Since a MT-SOFC is tubular it is expected that the trend described above will not be applicable. It will be the case that any onset of nickel oxidation will induce tensile stresses on the electrolyte and cathode. Thus, it may be that a MT-SOFC electrolyte will be less able to endure oxidation in comparison to the planar types. However, the mechanical strength of the planar and MT-SOFC geometries has not been compared and there may even be advantages in this regard to the small tubs. Since electrochemical oxidation and oxidation via fuel shortage or indeed oxidation via leeks are equally of concern. However, POX reforming conditions induced by leaked oxygen to the anode may simply negate these concerns. This aspect has been fundamentally unstudied in the literature.

Every subsequent red-ox cycle has an effect on the anode microstructure. Zhang et al. [163] have shown that Ni particles formed sub-sequential to the first reduction of the sintered NiO–YSZ sample are very large and coarse. A method for modelling anode oxidation specifically, "the degree of oxidation", is shown by Pihlatie et al. [85]. Currently, red-ox cycles studies in the literature concerning planar SOFCs, are state of the art and no in depth studies exist for MT-SOFCs. Moreover, to date, all studies have used inert gases containing oxygen in order to induce the oxidation. A much more realistic approach would be to perform studies whereby hydrocarbon fuels are used and the oxygen is somehow introduced to the fuel/anode like leeks at seals would occur. It should also be noted that electrochemical oxidation, most likely a result of fuel starvation, is a much faster damaging mechanism and would be expected to occur at the anode outlet; especially at high fuel utilisations. A rare example in the literature, Haut et al. [87], shows an equilibrium diagram where the tendency for carbon deposition or oxidation is shown when a hydrocarbon fuel is utilised. Most accounts in the literature focus on one event or the other. As additional information, on the theme of carbon deposition, the vast majority of carbon deposition related studies in the SOFC field do not consider whether anode oxidation would occur.

The extent of carbon deposition is largely governed by the relative kinetics of carbon formation and carbon removal reactions rather than by the reaction equilibrium. Indeed, work by Walters et al. [164] showed that the likelihood of carbon deposit formation depends strongly on cell temperature, current density, and residence time. Moreover, Walters et al. [164] indicated that although equilibrium favours deposit formation early in a tested channel case, the homogeneous finite-rate kinetics predicted relatively low levels of deposit precursors; due to limited residence time.

Equilibrium modelling assumes that the carbon depositing reaction kinetics are extremely fast [165,166], i.e. that the forward and reverse reactions are sufficiently rapid in order to establish equilibrium; but this is certainly not the case [167].

Moreover, because of the tiny fuel channel, MT-SOFCs will most likely be intolerant to carbon deposition. Should one of the MT-SOFCs in a stack become blocked, it may be impossible to regain flow through the cell. Furthermore, behind the carbon blockage, nickel oxidation will likely eventually occur. For a MT-SOFC stack, many ill advised scenarios can then occur including; exhaust gas flushing into the blocked cell and exhausting through cracks in the electrolyte, the blocked MT-SOFC damaging others as a result of its decreased OCV/short cuts or, indeed, pressure oscillations, which affect the overall stack power delivery stability. Effective strategies and procedures must be used in order to prevent carbon deposition in MT-SOFCs.

The re-oxidation and carbon deposition theme, despite its importance for the durability of MT-SOFCs, has not received adequate attention in the literature. For state of the art reviews regarding carbon deposition and other forms of SOFC hydrocarbon related degradation, the reader is referred to Refs. [52,167–169]. The state of the art is that detailed kinetic models for hydrocarbon fuels are computationally expensive, time intensive to validate and even the reaction data required for the numerous components and reaction paths in hydrocarbon fuels are unknown. Only time will tell how the modelling issues are resolved. Until then, it is expected that experimental measurements will guide experts to solutions in order to avoid carbon deposition or nickel oxidation.

5.2. Reports of MT-SOFC internal reforming systems

Pirelli Labs (S.p.A. Italy) [170] have been developing synthesis of ceramic composites by chemical routes (i.e. sol–gel, co-precipitation) that can be applied for anode, cathode or electrolyte components. From these technologies anodic nano-powders compositions were synthesised that were suitable to oxidise directly the CH_4 and bio-fuel. Acumentrics Inc. (USA) [171–173] in a selection of online presentations, give an insight into their various technologies including cells, stacks, production and some system design aspects. They also mention that they have products where their MT-SOFCs internally reform fuels [174].

Nano-Dynamics (Inc. USA) have very recently published a paper on internal reforming in MT-SOFCs. Cheekatamarla et al. [14] describe a MT-SOFC with a porous catalyst support membrane that was coated on the anode surface with a slurry containing active catalytic materials tailored according to the reaction chemistry. Fuel and air were supplied to the MT-SOFC anode facilitating partial oxidation. At oxygen to fuel ratios ranging from 1.06 to 1.6, fuel utilisation reached 60% and 40% respectively. In the paper, no information is provided detailing materials. However, it clearly conveys and demonstrates that MT-SOFCs partial oxidation reforming is possible. The importance of keeping the “oxygen/fuel ratio” close to stoichiometric values is also shown.

Cheekatamarla et al. [14] mention that an improvement in MT-SOFC power output was due to the anode, electrolyte and cathode optimisation. Significant anode and electrolyte microstructure improvements that facilitated lower mass-transfer resistance (higher porosity) and higher electric conductivity were pivotal optimisations. This is a very interesting clue regarding increasing a MT-SOFCs performance.

5.3. Reports using various fuels

5.3.1. Methane

Finnerty et al. [175] have described a catalytic measurement system, performed on a SOFC/MT-SOFC, using a mass spectrometer in order to continuously monitor the exhaust gas composition. Their study clearly showed that as the potential across the YSZ electrolyte is lowered, from the open-circuit voltage, there was increased methane conversion and stepwise hydrogen and CO production increase. Lower voltages caused an oxygen-ion flux increase across the solid electrolyte, from the cathode to the anode, and an increased SOFC current was drawn. The authors attributed the CO and H_2 production increase to a steam and dry reforming combination, direct electrochemical methane partial oxidation and the electrocatalytic carbon removal from the nickel anode mechanism. They attributed another factor causing the increased reforming to water and CO_2 production, through electrochemical oxidation of H_2 and CO. The increased water levels and some CO_2 apparently led to increased reforming activity and also increased carbon removal. Such measurement results and trends can also be found for planner SOFCs.

Interestingly, the authors [175] also discussed carbon removal from the anode during operation by switching off the fuel feed and observing the CO evolution in the exhaust. Kendall [47] discussed that this carbon deposition may in fact have some benefits for MT-SOFC performance. His group recommended, Bujalski et al. [28], that when methane, replacing hydrogen, was fuelled to the MT-SOFC, carbon deposition onto the nickel was observed and the likely cause of the test cells factor seven power increase observation. The explanation proposed was; that the methane deposited carbon onto the anode nickel particles, thus allowing them to make better electrical connection.

Also Buchinger et al. [130] investigated the methane concentrations in hydrogen that can be fed into a MT-SOFC by determining the cell performance over time. Also, the effect of adding water to the gas as a reforming agent was analysed with respect to power output and MT-SOFC stability. For example, in the case of dry hydrogen–methane blends, at 850 °C working temperature, it was found that up to a concentration of 10 vol% methane in the fuel was a possible fuel mixture for a MT-SOFC in the observed operation periods. Higher concentrations caused rapid cell power production degradation. Concerning these results, it seems that the SOFC with methane–hydrogen blends degradation effect is a combination of pore blocking and nickel/anode delaminating. Adding water allowed higher methane concentrations and increasing the temperature from 850 °C to 900 °C had positive stability effects when using hythane. The author also talks about nickel re-oxidation with higher steam concentrations. This was also discussed by Kendall et al. [176] where, especially in anode-supported cells, such reduction and oxidation cycles on nickel in the SOFC anode is very undesirable due to the stresses induced.

Recently Calise et al. [177] conducted a performance degradation experimental analysis regarding MT-SOFCs fed by hydrogen, carbon monoxide, water and methane in different ratios. The polarisation curves showed substantial performance degradation with pure hydrogen as fuel and with hydrocarbon fuel feeds. They attribute the degradation, when pure hydrogen was used, to crack formations and eventual delamination. The authors also indicated that they had electrical contact problems, which might have dominated the other degradation sources. Thus SEM measurements would be useful and are planned in order to substantiate their claims. When CO mixtures were fed to the MT-SOFC, degradation was also recorded. Degradation was lower when CH_4 mixtures were fed. Their results further substantiate that nickel based anodes can be detrimentally sensitive to CO and CH_4 exposure. Their ceria-based material only allowed carbon deposition delay, but ultimately failed to inhibit this phenomenon.

5.3.2. Wood gas

Regarding wood gas as fuel Buchinger et al. [129,178] investigated the maximum hydrogen chloride and hydrogen sulfide

impurities concentrations in synthetic wood gas. Electrolyte supported MT-SOFCs producing a 200 mA maximum current density was used at different working temperatures and flow conditions. It was found that operation with up to 50 ppm hydrogen chloride in hydrogen was possible, for at least time periods up to several tens of hours. Also stable cell performances could be observed with the combination of 10 ppm hydrogen chloride and 3 ppm hydrogen sulfide in the fuel. Wood gas from air gasification always led to a stable performance, but wood gas from a steam gasifier sometimes caused power degradation. Additionally, an impurity concentrations influence analysis during the MT-SOFC heating up and cooling down phases was performed.

5.3.3. Liquid based fuels

Fuelling a SOFC with liquid fuels such as methanol, ethanol, dimethyl ether, liquefied petroleum gas and carbon-free liquid fuels is examined by Cimenti and Hill [78]. They report that because of the lower propensity to form coke, methanol may be the optimal liquid fuel. They also report regarding anode design for hydrocarbon fuels, that there tends to be a balance between lack of carbon formation and sufficient electrochemical activity.

Kendall et al. [179] with MT-SOFCs have studied the theory that carbon–carbon bonds in the fuel are the main reason for anode damage. By testing a number of fuels in MT-SOFCs without such bonds, particularly liquid ethers such as methyl formate and dimethoxy methane, they showed that SOFCs can run without substantial carbon formation. Out of the almost 100 molecules and formulations tested, a wide range of electrical performance data was recorded. Certain molecules like glycerol and *N*-methyl methanamide gave a rapid drop in current with time when injected directly onto the nickel cermet anode. Other molecules like methanoic acid gave performance similar to hydrogen, showing nearly steady current with time over periods of several hours. From these experiments, it was clear that certain molecules like methyl formate gave much less anode damage than expected in SOFC operation.

When used directly in SOFCs, certain molecules with no C–C bonds deposited less carbon on a nickel cermet anode than their carbon content would suggest. In particular, methyl formate and dimethoxy methane can produce very little carbon deposition when injected directly into a MT-SOFC, especially in the presence of water and methanoic acid. When blended with water and methanoic acid, electrical performance was comparable to that of hydrogen, carbon deposition was reduced to negligible levels.

5.4. MT-SOFC materials and internal reforming

Reports of groups in the MT-SOFC field using alternatives to nickel in the anode are seldom. Direct exposure of hydrocarbon fuels to the conventional nickel based anodes has been problematic due to their high catalysis for hydrocarbon cracking reactions at the operating temperatures, leading to carbon accumulation in the anode and thus eventually degrading the cell performance [180]. Kendall, in his review paper [104], discussed, in the anode section, several limitations and problems found in the literature. He also discusses some alternative materials, briefly stating that apart from nickel cermet, candidate anode materials have not fulfilled their early promise. For example, LaSr-chromite [52]. Ce doped $SrTiO_3$ can be readily oxidised. Cu/CeO_2 cermets are useful for direct operation on hydrocarbons but acceptable operation has been difficult to repeat. Some transition metal (Cr, Mn, Fe) perovskites may eventually show useful properties. Although, alternative anodes that allow the operation of SOFCs directly on hydrocarbons have been developed, hitherto, there are still some problems associated with all the alternative materials, mainly low catalytic activity [77].

Only changing the anode material will not optimise MT-SOFC performance with hydrocarbon fuels. Zhan and Lee [180] show, for example, when copper anodes are used other materials in the cell should also be changed to optimise the cells performance. For example, the substitution of SDC, a mixed ionic and electronic conductor, for YSZ in the copper anode resulted in increased maximum power densities, to 0.35 W cm^{-2} for hydrogen and 0.22 W cm^{-2} for propane in comparison to CuO–YSZ–ceria anodes whereby 0.26 W cm^{-2} and 0.17 W cm^{-2} were recorded in hydrogen and propane, respectively. Impedance analysis revealed that the anodic polarisation resistance for CuO–SDC–ceria in hydrogen was much lower than for CuO–YSZ–ceria, e.g., 0.2 Ω cm^2 vs 0.7 Ω cm^2 at 800 °C. The relatively high cathodic polarisation resistance of 0.5 Ω cm^2 at 800 °C in the LSM–YSZ cathode-supported SOFCs suggests that it is critically important to optimise the chemical composition and porous microstructure of the cathode substrates in order to further improve the cell performance.

6. Reported alternative MT-SOFC modes of operation

6.1. Single-chamber SOFC

Single Chamber (SC-SOFCs) is an interesting SOFC evolution. Conventionally SOFCs provide a separated fuel and oxidant channels on either side of the electrolyte. The SC-SOFC on the other hand has a single channel, where the oxidant and fuel are utilised in the electrochemical reactions, either by selective materials or by selective geometries as seen in Fig. 4. A comprehensive SC-SOFCs review, up to 2007, is provided by Yano et al. [181]. The authors indicate that such devices have relatively low fuel efficiency and this is a major challenge. At present fuel oxidation and oxygen reduction selective anode and cathode materials are not available. Furthermore, SC-SOFC design optimisation requires attention. The authors state that SC-SOFCs could provide a performance comparable to conventional SOFCs. But the realisation of this goal seems some way off, if it is even possible. Moreover, some new avenues of SC-SOFCs for various applications are proposed on the basis of; cell designs, thermal properties, and fabrication processes.

Prof. Kendall's group [182,183] are pioneering micro-tubular, single-chamber solid oxide fuel cell (MT-SC-SOFC) development. Akhtar et al. [183] have studied four different MT-SOFC cases with varying cathode location/size, i.e. inlet, centre, outlet and full size in order to establish cathode location and temperature effects. The study showed that the highest temperature rise of 93 °C (at a furnace temperature of 750 °C with methane/air equal to 5/60 mL_N min^{-1}) was observed, when the cathode was located at the MT-SC-SOFCs inlet. Furthermore, it was observed that the cell inlet is more damage sensitive, since large exothermic heat generation existed. This heat generation was attributed to fuel oxidation directly at the anode inlet. The cathode-outlet configuration caused relatively lower temperature gradients since the electrical power generation at the outlet raised its temperature closer to the level of the reforming influenced inlet temperature. Their study demonstrated that continuous excess heat generation, attributable to reforming or combined reforming and power generation, will cause local hot spots provoking structural damage, particularly at the MT-SC-SOFC inlet. Moreover, the inhomogeneous temperature distributions and stark temperature gradients along the MT-SC-SOFCs length can evoke a mechanical compression and tension state. The MT-SC-SOFCs power density was also highly non-uniform, attributable to a temperature induced large electrolyte ionic conductivity variation. Akhtar et al. [183] stated that while it is generally believed, within the field, that exothermic heat is advantageous, in order to lower the external heat demand, the negative effects have been disregarded. Since many practical

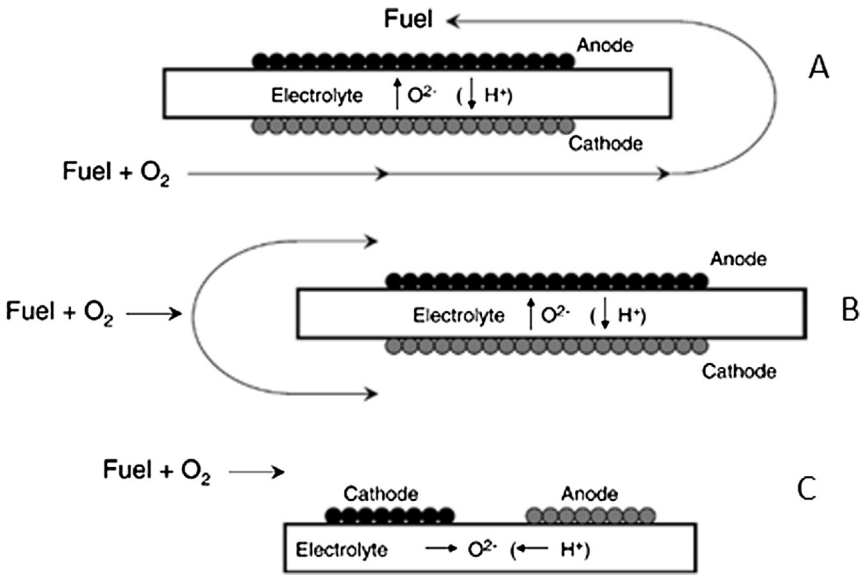

Fig. 4. Principle of single channel SOFC operation [184] where "A" shows a cathode then anode reaction flow path where the electrodes are on either side of the electrolyte, "B" shows a flow splitting regime where the electrodes are on either side of the electrolyte and "C" shows a similar flow regime to "A" but with the electrodes on the same side of the electrolyte.

hydrocarbon fuels produce even larger excess reaction heat quantities than the methane studied, signs of early SC-SOFC degradation and structural damage cannot be afforded.

Akhtar et al. [182] have developed a two-dimensional, axi-symmetric, MT-SC-SOFC numerical model. The model considered, methane full combustion followed by methane steam and dry reforming considering the water-gas shift reaction producing additional hydrogen. The cathode side included methane parasitic combustion and oxygen electrochemical reduction consideration. The results established that MT-SC-SOFC's poor performance, when compared to conventional (dual-chamber) MT-SOFC, is related to an anode side mass transport limitation. They report that gas velocity inside the micro-tube is far lower than that at the gas-chamber inlet. Furthermore, the current density along the cell length was highly non-uniform, suggesting that the anode current collection should be made throughout the anode length or the cell length must be shortened in order to make the current density as uniform as possible. The calculated and measured temperature profiles in Ref. [183] are in good agreement, indicating the appropriate selection of anode side chemistry. With the aid of calculated performance curves, the model was validated against their earlier experimental study [183]. The results show that the model is able to predict the experimental trends and is reliable for optimisation of the experimental setup. The MT-SC-SOFC is currently in the feasibility stage and will remain so until its fuel conversion efficiency increases drastically.

6.2. Steam electrolysis

A SOFC having the ability to function in Solid Oxide Electrolyser cell SOEC mode is of interest. Such a device could be used in order to produce hydrogen or syn-gas for storage, which could later be used by the same device to produce power. A recent study has shown the long term SOEC durability depends, to a large extent, on the purity of the gas supply [184]. MT-SOFC reversible operation with high electrochemical efficiency was demonstrated by Laguna-Bercero et al. [185]. The MT-SOFC reverse configuration, Solid Oxide Electrolyser (MT-SOE) can produce hydrogen using electricity and water vapour. The stored hydrogen can then generate electricity and heat. An anode-supported Ni–YSZ/YSZ/$La_{0.8}Sr_{0.2-0.98}MnO_3$ SOFC, having a 2.4 mm diameter and 20 μm electrolyte thickness was manufactured. The MT-SOFC electrolysis mode was analysed as a function of fuel channel steam concentration. At 850 °C, the cell endured current densities of −1 A cm^{-2} at 1.3 V while the steam utilisation was 16.5%, measured by mass spectrometry. *I*/*V* curves showed an S-shaped non-linear behaviour. In the electrolysis mode, saturation at high current density values was observed. The cell sustained −6 A cm^{-2} current density at 1.5 V, using 70% H_2O, 15% H_2 and 15% N_2 as the fuel. This MT-SOFC performance in the SOE mode is very promising regarding MT-SOFC high-temperature electrolysis applications. However, much more work is required in order to establish the feasibility and durability of a reversible MT-SOFC.

7. Mechanical properties of cells

7.1. Experimental reports

Studies examining MT-SOFC mechanical properties are quite rare. Fundamentally, it seems that mechanical concerns are not constrictive in this MT-SOFC early development phase. Should MT-SOFCs be applied in situations, where mechanical shocks, vibration or experience habitual shut-down and start-ups occur, mechanical optimisation and targeted consideration will be obligatory. Regardless, the available accounts in the literature provide an interesting insight regarding MT-SOFC mechanical stability.

A drop test reported by Kendall [47] and performed by Adaptive Materials Inc. showed that a MT-SOFC stack can be plunged from 1 m and incur no damage. This test indicated that a MT-SOFC stack can withstand single robust shocks. However, no vibration or multiple drop tests have been reported, to date. It is known that decreasing the thickness or increasing the electrolyte conductivity enables lower temperature SOFC operation. Reducing the overall MT-SOFC wall thickness has additional benefits. Features, such as low thermal mass and thermal shock resistance enable rapid SOFC start-up and shut-down time. However, when the SOFC wall thickness is reduced, its mechanical strength diminishes. Thin-walled tubular SOFCs tend to be relatively fragile hindering self-

supporting. This limits their usefulness in products, especially in conditions that require robust fuel cell components. Various exemplary fuel cells, electrodes and methods are presented in Ref. [186] that indicate solutions for SOFCs that can withstand or minimise induced stresses.

Prof. Kendall's group have made some studies regarding MT-SOFC thermal cycling ability [28,126,187]. In a recent contribution to the field, Kendall and Dikwal [187], the group compare thermal and red-ox cycles. They discuss how partial oxidation is less damaging than full oxidation and indeed that thermal cycling is far less damaging than oxidation cycling. It is suggested that the first few MT-SOFC thermal cycles are the most damaging. Their explanation for the thermal cycling induced MT-SOFC performance reduction is that each cycle precipitates micro-cracks within the anode cermet. This marginally separates the nickel particles and causes extra anode electrical resistance. They support this theory with dilatometric measurements [176], which showed that the cermet expanded irreversibly after each cycle. During each cycle the micro-cracks extended equally. This is stated because the crack driving force is relaxed by the expansion process and relates to a fatigue equation. What the group also show is that after 30 thermal cycles the MT-SOFC performance did not reduce significantly. The red-ox cycled MT-SOFC performance stabilised after 10 s of cycles. Interestingly the red-ox caused damage was much worse than the damage caused by thermal cycles. This was indicted by large cracks and indeed electrolyte delamination. Kendall and Dikwal [187] also pointed out that red-ox cycling is most damaging at low ramp rates while thermal cycling damage is milder. Therefore there is an optimum MT-SOFC cycling rate in cases when the fuel is interrupted.

Roy et al. [188] have indicated that after SOFC reduction, a wall thickness decrease can cause a MT-SOFC hoop strength increase and that a porosity increase yields a strength decrease. Mohammadi et al. [189] showed that the average fracture strength on NiO–YSZ samples increases until the third red-ox cycle and then levels off at the fourth and fifth cycles. Hoop stress is mechanical stress defined for rotationally-symmetric objects being the result of forces acting circumferentially, perpendicular both to the axis and to the radius of the object. However, it can clearly be seen in Refs. [188,189] that mechanically testing these materials is very capricious as samples; identically sintered, treated and tested can give erratic results.

Moreover such experiences regarding ceramic and cermets this is not unusual. The flaws in most ceramics are statistical in nature. Thus a ceramic's strength is not one specific value, rather a distribution of strengths. The Weibull modulus, for example, is a measure of the flaw distribution, usually for a brittle material. The modulus is a dimensionless number corresponding to the variability in measured strength and reflects a material's flaw distribution. For brittle materials, the maximum strength (stress that a sample can withstand) varies unpredictably from specimen to specimen as seen in Refs. [188,189] even under identical testing conditions. Thus a statistical analysis with abundant samples is imperative.

Roy and Sammes [190] investigated MT-SOFCs mechanical properties. Internal burst testing and monotonic compressive loading on MT-SOFC C-ring test specimen was performed. The burst test is an important parameter because improved power efficiency at increased fuel pressures is possible [191]. Furthermore, C-ring testing is critical in order to determine ultimate strengths. They made baseline cells with 40% pore former, sintered at 1400 °C with a 314 μm anode wall thickness. Baseline variations were 60% pore former, sintering temperature decrease to 1350 °C and a wall thickness reduction to 230 μm. Again erratic mechanical results were recorded. Hoop stress axial stress and radial stress comprise the stress tensor in cylindrical coordinates. The authors pointed out that, even considering the large result scatter percentage and mechanical testing method contradictions, it seemed apparent that increasing the pore former or decreasing the sintering temperature caused a hoop stress decrease. Moreover, decreasing the wall thickness increased the hoop stress.

Galloway and Sammes [123] found that after load-cycling testing the MT-SOFC performance was degraded in both loaded and OCV conditions, where the worst degradation occurred during the first day of operation. The cycles were simply performed over the duration of a week whereby, during the OCV test the cell was loaded once per day in order to make recording and the loaded case involved a cell that was permanently loaded at about 0.4 A cm^{-2} and unloaded once per day in order to make OCV measurements. This kind of degradation is a serious issue regarding MT-SOFC application. Environmental scanning electron microscope (ESEM) analysis showed that there was a porosity decrease in the degraded MT-SOFC anodes that prevented fuel from arriving at the reaction sites.

7.2. Simulation reports

Serincan et al. [192] presented a detailed mechanical MT-SOFC model investigation subjected to thermal stresses analysis. The stresses considered arose from MT-SOFC fabrication, exterior constraints, and MT-SOFC operation. Considered fabrication stresses only included stresses induced during MT-SOFC sintering. The authors pointed out that if the support conditions are chosen carefully, an operating MT-SOFC is not exposed to stresses as high as the residual stresses at room temperature. The authors show that a large section of the anode, sealant and alumina tube are in tension, whereas electrolyte is in compression. Residual stresses determine the overall stress field within the bulk MT-SOFC layer, while the cell and the support structure interactions have significant stress distribution effects. Electrolyte regions that are not covered with a seal or cathode layer, do not have the added cathode radial constraint. Therefore, these regions tend to freely expand more than the other regions. Moreover, the zone between the two seals at either MT-SOFC end may experience a warping effect.

Underneath the ceramic seals, attaching the MT-SOFC to the manifold, a dual trend was noticed by Serincan et al. [192]. Where there existed a compressive contribution to the overall axial stress in the MT-SOFC end seals, principally at the seals outmost location, please refer to Fig. 5. The large seal and electrolyte thermal expansion coefficient mismatch is stated as being the cause. The electrolyte tensile stress, located at regions closer to the MT-SOFC active region, is suggested to arise because, in the nearby zone, uncovered by the ceramic sealant, the MT-SOFC was free to move in the axial direction. Bishop et al. [193] have furthermore indicated that low oxygen concentrations may induce stresses in ceria and GDC electrolytes that would only occur at significant lower oxygen concentrations in YSZ electrolytes. Generally MT-SOFCs are much longer than the one shown in the model of Serincan et al. [192] and thus realistically, the axial stress may be larger than that modelled in their case.

Cui et al. [194] neglected the interaction between the MT-SOFC sealing and housing in their model. However, they agree with the result of Serincan et al. [192], that overall, the electrolyte experiences compression. Cui et al. [194] also showed via their model that the cathode is also under compression, while the anode endures tensile forces. Mariani [195] simulated MT-SOFC anode stresses where temperatures, that vary from the front and back of the cell and variable temperature conditions along the MT-SOFC length, are also considered. A very interesting finding in this paper is that the oxidant channel design is quite important. Mariani [195] showed that when a 27 K gradient exists across a MT-SOFC front and back, a

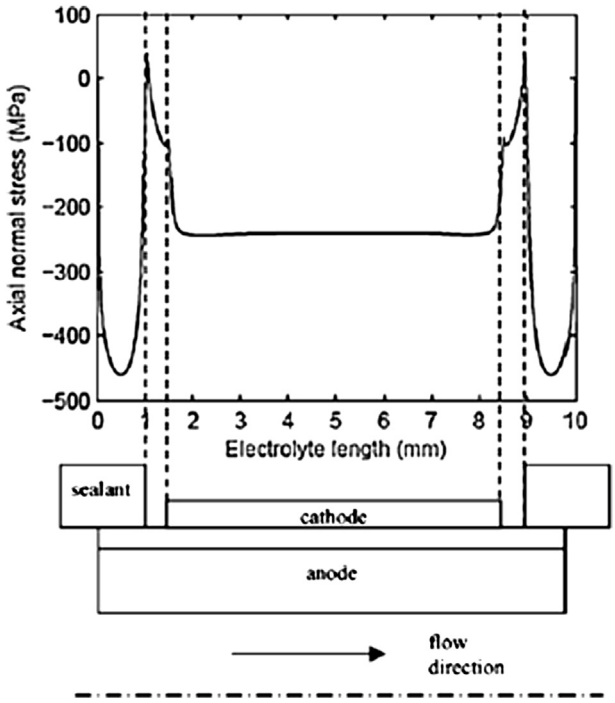

Fig. 5. Axial normal stress profile along the electrolyte centre line. Please refer to Serincan et al. [192]. Note the location of the maximum axial stress in relation to the sealant and cathode.

von Mises stress of 231 MPa can exist. In contrast a thermal gradient longitudinally along the MT-SOFC resulted in a von Mises stress of 4.9 MPa.

Cui and Cheng [196] for a slightly lower temperature gradient showed that the anode tensile stress is still below 7 MPa. They also recommend that the anode will most likely be the first cell material to fail and furthermore recommend that in order to relieve stresses between the individual MT-SOFC components, the anode Coefficient of Thermal Expansion (CTE) is probably the most important to rectify. Moreover they recommend maintaining a slow sintering temperature rate during SOFC manufacture, especially at high temperatures. This is because the stress is smaller close to the stress-free temperature. Many uncertainties remain in this area. A thin film of the YSZ electrolyte was deposited on the anode tube at a temperature of 1723 K. At this temperature both the anode and the electrolyte film are described as stress-free in their present work. A LSM/YSZ composite cathode is fired on the YSZ film at 1523 K. At this temperature the cathode is supposedly stress-free.

A limitation of the models of Mariani [195] and Cui and Cheng [196] is that the porous microstructure is not considered, which may have some effect. Serincan et al. [192] reported a 570 MPa compressive stress in the electrolyte and Cui and Cheng [196] 270 MPa. The result variation can arise, when considering the different temperatures and MT-SOFC geometries that were modelled.

7.3. Mechanical feature analysis and methods

Blum et al. [197] used a combination CFD and FEM in order to establish why their large planar SOFC stacks developed leeks during operation. Experimental analysis consisted of the building of stacks that replaced the planar SOFCs with metal sheets. Experimental measurements were recorded using thermocouples in order to validate CFD models. The values predicted and validated by these simulations were subsequently exported to FEM software. A novel approach, whereby a dye was used in order to isolate cracks and a FEM analysis, indicated that high tensile stresses caused by gas induced stack temperature variation caused the cracks. Such an FEM analysis allowed this group to isolate exactly what are the tolerable tensile stresses for their sealing materials. Furthermore, the CFD analysis, considering previous FEM analyses, allows the designers to design the stack manifold and gas distribution effectively in order to avoid excessive temperature gradients.

Simplified sequential approaches that have been previously demonstrated by SOFC designers [195,197] are extremely useful and relatively simple to achieve. The fact that the SOFC stack geometries change by small values, during operation, means that the CFD predicted temperature profiles can be exported to FEM analysis software. In other words, the stack shape does not change to the point whereby a further CFD analysis would be required in order to describe the fluid dynamics. This fact means that a single iteration of combined CFD and FEM approach applied to MT-SOFC stacks combined with either structural fault indication via the dye approach [197] or non-destructive Computer Tomography (CT) for validation may provide sufficient information as a basis to improve stack designs. This approach applies to both conventional and MT-SOFC stack designs.

Griesser et al. [198] have studied the potential of X-ray tomography as a potential non-destructive testing platform for analysing single MT-SOFC cells and stacks. They used this technology to analyse the connection of a nickel mesh current collector inside an electrolyte supported SOFC with excellent visual results. The method was also used to find holes in seals within stacks. This is a very useful albeit expensive technology concerning non-destructive MT-SOFC current collection contact, stack manifold and seal analyses.

Lawlor [199] has indicated that there is a lack of critical measurement data which generally not available for SOFCs. Namely, temperature measurements recorded at within the SOFC during operation. While such measurements are surely very difficult to perform without disturbing the temperature field, some measurements are required in order to validate the temperature profile measurements and subsequently any stress predictions. The lack of such measurements required by modellers will require some very innovative and challenging measurements from experimentalists. The MT-SOFC and a smart use of its geometry may provide a platform for a novel experimental apparatus in order to achieve such measurements. Qualitative measurements may even be the most that can be achieved, but without any data in the literature of any kind if measurement would be state of the art.

8. Diagnosis and quality assurance

For MT-SOFCs to become commercially available, like other forms of fuel cells and indeed traditional SOFCs, they must be readily tested and improved. In the literature there are relatively few accounts detailing standardisation or optimisation of testing procedures or even articles discussing this theme. The following section investigates reports regarding standard procedures reported in the SOFC field and furthermore highlights some interesting accounts of measurements relevant to MT-SOFC developers. Degradation is currently a very important theme as can be extrapolated from the types of EU and DOE projects being recently funded.

It should be noted that the reliability, standards and testing theme deserves a review paper dedicated to this topic alone and the following section points out some critical aspects.

8.1. Measurements and standards

Feasibility of SOFC technology as a power providing device for the open market has more or less been proven. However, the

durability and reliability of this technology is a different issue and is of serious concern. The lifetime of SOFC systems for stationary systems will have to be about 40,000 h while for automotive application 5000 h will be expected [88]. MT-SOFCs could be considered for both applications. Testing over a period of 40,000 h is neither practical nor is it efficient or arguably necessary. Thus MT-SOFC companies will have to rely upon accelerated testing methods in order to establish the reliability and durability of their technology [88]. Testing of individual planar SOFCS is expected to be much more expensive in comparison to MT-SOFCs owing to the price of appropriate manifold and housings. In this regard MT-SOFCs would have an advantage since relatively inexpensive ceramic pipes are readily available. However, product stack manifold and housing bring their own unique challenges to both designs as discussed in Part I of this review [46].

Gemmen et al. in a quite unique article [200], discuss some critical aspects regarding SOFC performance/degradation measurement technique issues and propose methods in order to establish degradation in fuel cell systems. Gemmen et al. [200] state that various advances in the SOFC field have reduced degradation rates to less than 1% per 1000 h. The implication for developers with mature SOFC/MT-SOFC technology is that measuring performance improvements, due to incremental changes in design or materials, can be difficult and expensive owing to the increased data sensitivity requirements and/or extended test period durations. Apparently, statistically significant resolution of the differences between two cell designs requires thousands of hours of intricate testing. The authors Gemmen et al. [200] highlight an anomaly in testing procedures, which may not be obvious to the general field. In Fig. 6 the time required to resolve (to within 25%) the true degradation of a cell as a function of the degradation rate is shown from Ref. [200]. The degradation rate was calculated as the difference in the starting and finishing voltages. An experimental noise of 3 and 1% was considered while the standard error in the degradation rate was 25%. The results clearly indicate that a reduction in experimental noise is required in order to reduce the amount of time required in order to assess the degradation.

The significance of this observation is that since experimental noise is largely fixed, as technology improves and degradation is decreased, longer test durations are required to accurately measure the true degradation. Aside from electrical instrumentation noise, other primary sources of noise and “SOFC operation variation” are experimental temperature, pressure and reactant concentration will cause noise. A degradation performance parameter (or parameters)

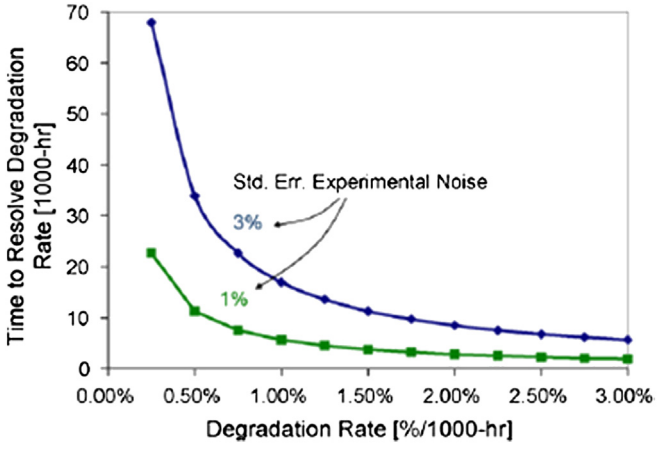

Fig. 6. Time to resolve the degradation rate as a function of the degradation rate (Gemmen et al. [200]).

that mitigate the influence of such experimental ‘noise’ on the degradation measurement is needed and some are suggested by Gemmen et al. [200].

In their work, as an example, they suggest OCV monitoring would be suited as a reference for work focused on electrode-to-electrode performance comparisons, and would remove voltage loss effects attributed to seal leaks. On the other hand, by using the ideal potential as a reference, the effects of seal degradation (e.g., leakage) over time can also be captured in the ASR data, which is important for stack level studies.

Haanappel and Smith [201] have published a review concerning SOFC measurement and quality assurance standardising at Forschungszentrum Jülich (FZJ). They provide an insight regarding the FZJ standardisation structure and SOFC monitoring. Testing at FZJ is consecutively categorised and presented in a flowchart context. This chart follows standard conventions, describing the process initialisation, outlines critical parameters, indicates possible decisions, has feedback loops concerning non-conformal situations and specifies the information to be collected and how/where it is to be recorded.

The authors suggest that SOFCs from different manufacturers behave differently. Hence, the actual values manufacturers described are meaningless for other developers. In all modern manufacturing branches and the service industry, systems are enforced ensuring the product output quality. As SOFC technology approaches mass manufacture, necessarily, such systems need to be designed in order to guarantee the product quality and present a professional image. Moreover, for the developer, adapting such systems provides marked advantages in all SOFC development stages. Such systems represent a formalised enforcement criterion that ensures best scientific and engineering practice. The account of Haanappel and Smith [201] was the only significant published SOFC quality assurance system account found in the literature and the rest of this section will focus on measurement techniques, which could and should be integrated into such standardisations also for MT-SOFCs.

8.2. Reports of MT-SOFCs and EIS measurement

The physicochemical processes fundamentally driving a SOFC can be classified in two ways [202]. Firstly, as internal factors, including material, composition, microstructures and component sizes, or secondly as external factors, including temperature, pressure, and fuel/air flows and concentrations. Measured impedances give information detailing the reaction kinetics, reaction activation, electrolyte conductivity, mass transfer, and operation conditions, allowing SOFC performance and failure modes diagnosis [202]. Such diagnosis facilitates fuel cell performance improvement through the agency of design and component optimisation.

In SOFC AC impedance measurements, a perturbation voltage signal with an amplitude ranging from 10 mV to 50 mV is normally selected with a frequency range of 0.01 Hz−1.0 MHz [202]. The shapes of the impedance plots reflect the coupling of many SOFC factors and parameters. Through targeted experimentation based upon parameter variation and equivalent circuit modelling, useful information concerning the material composition, microstructure, and operation conditions is obtainable. The reader is pointed to the review paper of Huang et al. [202] for a detailed introduction regarding SOFCs and EIS. The following account relates specifically to measurements made regarding MT-SOFCs.

A MT-SOFC impedance study has been performed by Nakajima et al. [203]; where the authors discuss many important EIS measurement features. For example the effect of cathode oxygen partial pressure, effect of hydrogen partial pressure and effects on the equivalent circuit modelling is discussed and explicitly detailed. The variations in the equivalent circuit parameters, for the charge

and mass transfers at the anode and cathode and ohmic resistance under operation condition, were obtained separately. Furthermore, the average diffusion length associated with the anode Nernst loss was estimated. Monitoring these parameters allowed separated electrode, gas feed, electrolyte and current collector diagnostics. This enables degradation detection and abnormal operating conditions, which can pre-empt serious failures.

In a novel account, Soderberg et al. [93] have compared a MT-SOFC to a planar SOFC via impedance measurements. Their similar polarisation resistance values, regarding LSM–YSZ oxygen reduction reaction activity, concerning both the micro-tubular and planar cell geometries indicated no significant geometry effect. Furthermore, their SOFC electro-phoretic deposition fabrication method also appeared to incur negligible effect. In particular, an excessively thick cathode functional layer should yield a larger polarisation resistance and their result showed that sintering the MT-SOFC LSM–YSZ cathode at 1150 °C vs 1100 °C yielded a higher oxygen reduction reaction activity, a consequence of a lower polarisation resistance. Lower polarisation resistance values were obtained for LSM–YSZ sintered at 1150 °C (0.7 Ω) compared to at 1100 °C (1.6 Ω). While the high frequency constant phase element values were the same for both sintering temperatures ($\sim 3.5 \times 10^{-2}$ F cm^{-2}), the low frequency constant phase element value was twice as high for LSM–YSZ sintered at 1150 °C ($8 \pm 2 \times 10^{-2}$ F cm^{-2}), compared to 1100 °C ($4.5 \pm 0.5 \times 10^{-2}$ F cm^{-2}). As the polarisation resistance decreased from ∼2.5 to ∼1.3 Ω cm^{-2} for the 1150 vs 1100 °C material, the "polarisation resistance" and "constant phase element" product was relatively constant. The authors recommend that this indicated no catalyst material inherent property change and that only the total active three phase boundary length was increased. This suggests that the higher cathode sintering temperature improved the bonding between the electrolyte layer and the cathode as well as the particle/particle contact within the cathode layer itself. The study of Soderberg et al. [93] is an exemplary account concerning EIS use as an MT-SOFC material optimisation tool.

Suzuki et al. [124] prepared two different MT-SOFC anode substrates. The anode tube for MT-SOFC sample "A" was prepared using NiO (dg∼5 μm) (dg = particle grain diameter) and GDC (dg∼0.2 μm) powders without using a pore former, while the anode tube for MT-SOFC sample "B" was prepared using NiO (dg∼0.5 μm) and GDC (dg∼0.2 μm) powders using a pore former. The authors found, from the high frequency intersection in the impedance spectra, that the ohmic resistances for MT-SOFC "A" and "B" were almost identical, 0.5 Ω cm^2. However, the electrode polarisation impedance of the two cells was significantly different. Therefore, the larger impedance arc of MT-SOFC "A" was mainly due to the lack of catalytic activation and fuel gas diffusivity at the anode side. On the other hand, the MT-SOFC "B" 50 wt-% NiO-50 wt-% GDC anode composition significantly improved the electrochemical performance. This is attributed to anode reaction rate enhancement a consequence of MT-SOFC "B"'s anode layer catalytic activity and gas diffusivity.

Galloway and Sammes [123] used impedance measurements in order to study MT-SOFC degradation. The information gathered through the impedance analysis showed that the entire MT-SOFC impedance decreased the longer it operated. The load-cycling was used in order to test the performance of the cells and this is described in Section 7.1.

ESEM analysis showed that there was a decrease in porosity in the anodes of the degraded cells that prevented fuel from arriving at the reaction sites of the MT-SOFC. EIS measurements showed that the MT-SOFC specific resistance remained relatively constant at approximately 0.5 Ω cm. However, the electrode polarisation resistance decreased with time, until after approximately 50 min no further electrode polarisation resistance change was observed, as a function of time. Initially the electrode polarisation resistance decreased by as much as 0.25 Ω cm in 10 min. The authors state that the electrode polarisation impedance curve changes suggested that the MT-SOFC would not reach peak performance until 50 min after start-up.

Buchinger et al. [204] using EIS and electrolyte supported MT-SOFCs found that the power density increase caused by cathode activation at the beginning was compensated by an increase in anode resistance due to too low nickel content, which lead to nickel agglomeration. This finding allowed the group to increase the performance of ESCs to 440 mW cm^{-2} at 0.7 V and 900 °C with hydrogen as fuel.

Additional to this, Buchinger et al. [204] reported a huge increase of the losses associated with the anode that was found with ongoing operation. After about 290 h the lower frequency semi-arc showed a much higher diameter compared to the spectra measured after 150 h. In accordance to this, the maximum power output of this cell also decreased from 175 mW cm^{-2} to 116 mW cm^{-2} (1173 K, 50 ml$_N$ min^{-1} hydrogen with 3 vol% water) during a time period of about 140 h. Reports of similar occurrences for ASCs were also reported in this study.

Campana et al. [120] using EIS techniques and an equivalent circuit model, which separated the different cell components contributions to the polarisation loss. The most important conclusion was that during cathode fabrication Mn loss should be avoided. Manganese evaporation is more noticeable when cathode thickness is small and sintering temperatures are high. This is an interesting observation most easily observed through EIS measurements.

9. Conclusion and recommendations

This review paper has gathered state of the art information regarding MT-SOFCs. Some background information useful to those new to the field, materials, manufacture, architectures and geometries and degradation durability and reliability issues was researched. The state of the art would suggest that anode, cathode and electrolyte supported MT-SOFC development is only slightly behind the comparable SOFC status. Durability and reliability is, to some degree, being driven by tests being performed on larger SOFCS, this would seem the case; at least from reports in the open literature. Cases considering MT-SOFC durability and reliability are not prevalent in the open literature. Apart from the hype surrounding the thermal cycle capability of single cells successfully durability has not been established. It is likely the case that the companies involved would have the resources and drive to establish durability and until "success stories can be told" reports will likely be scarce. Accelerated testing of MT-SOFC cells will be key to their rapid development. In particular, durability when fuelled with hydrocarbon will require much more attention in the MT-SOFC field and the severity of the consequences related to carbon deposition have not yet been considered or tested.

With regard to the next generation of SOFCS i.e. the metal supported type, the MT-SOFC has not been developed or considered to any significant degree. The reason for this is not clear and several methods in order to produce metal supported MT-SOFCs have been discussed in this review. Furthermore, MT-SOFCs in SOEC mode or SC mode are also sparsely covered in the literature.

References

[1] A.J. Appleby, Energy 21 (1996) 521–653.
[2] D. Gieleten, G. Simbolotti, Prospects for Hydrogen and Fuel Cells, Energy Technology Analysis, OECD Publishing; International Energy Agency, 2005.
[3] S.C. Singhal, K. Kendall, High-temperature Solid Oxide Fuel Cells: Fundamentals, Design and Applications, Elsevier Advanced Technology, Oxford, 2003.

[4] T. Suzuki, Y. Funahashi, T. Yamaguchi, Y. Fujishiro, M. Awano, J. Alloys Compd. 451 (2008) 632–635.
[5] T. Misono, K. Murata, J. Yin, T. Fukui, ECS Trans. 7 (2007) 1355–1361.
[6] T. Yamaguchi, T. Suzuki, Y. Fujishiro, M. Awano, S. Shimizu, J. Fuel Cell Sci. Technol. 7 (2010) 041001–041004.
[7] M.H.D. Othman, Z. Wu, N. Droushiotis, G. Kelsall, K. Li, J. Memb. Sci. 360 (2010) 410–417.
[8] C. Sun, R. Hui, J. Roller, J. Solid State Electrochem. 14 (2010) 1125–1144.
[9] B. Liu, Y. Zhang, J. Univ. Sci. Technol. Beijing Mineral Metall. Material 15 (2008) 84–90.
[10] M. Liu, D. Dong, R. Peng, J. Gao, J. Diwu, X. Liu, G. Meng, J. Power Sourc. 180 (2008) 215–220.
[11] A.K. Sleiti, J. Power Sourc. 195 (2010) 5719–5725.
[12] A.K. Sleiti, in: Proceedings of ASME 2008 Summer Heat Transfer Conference, HT2008-56447, Jacksonville, Florida, USA, 2008.
[13] P.K. Cheekatamarla, C.M. Finnerty, J. Cai, Int. J. Hydrogen Energy 33 (2008) 1853–1858.
[14] P.K. Cheekatamarla, C.M. Finnerty, Y. Du, J. Jiang, J. Dong, P.G. Dewald, C.R. Robinson, J. Power Sourc. 188 (2009) 521–526.
[15] O. Smorygo, V. Mikutski, A. Marukovich, Y. Vialiuha, A. Ilyushchanka, N. Mezentseva, G. Alikina, Z. Vostrikov, Y. Fedorova, V. Pelipenko, R. Bunina, V. Sadykov, Int. J. Hydrogen Energy 34 (2009) 9505–9514.
[16] R.J. Gorte, H. Kim, J.M. Vohs, J. Power Sourc. 106 (2002) 10–15.
[17] M. Stelter, A. Reinert, B.E. Mai, M. Kuznecov, J. Power Sourc. 154 (2006) 448–455.
[18] Y. Mizutani, K. Hisada, K. Ukai, M. Yokoyama, H. Sumi, J. Fuel Cell Sci. Technol. 2 (2005) 179–185.
[19] F. Calise, M. Dentice d'Accadia, A. Palombo, L. Vanoli, Energy 31 (2006) 3278–3299.
[20] D. Cocco, V. Tola, Energy 34 (2009) 2124–2130.
[21] R. Kandepu, L. Imsland, B.A. Foss, C. Stiller, B. Thorud, O. Bolland, Energy 32 (2007) 406–417.
[22] F. Calise, M. Dentice d'Accadia, L. Vanoli, M.R. von Spakovsky, Energy 32 (2007) 446–458.
[23] Y. Komatsu, S. Kimijima, J.S. Szmyd, Energy 35 (2010) 982–988.
[24] M. Burer, K. Tanaka, D. Favrat, K. Yamada, Energy 28 (2003) 497–518.
[25] M. Santin, A. Traverso, L. Magistri, A. Massardo, Energy 35 (2008) 1077–1083.
[26] G.D. Agnew, D. Bernardi, R.D. Collins, R.H. Cunningham, J. Power Sourc. 157 (2006) 832–836.
[27] S. Farhad, F. Hamdullahpur, Y. Yoo, Int. J. Hydrogen Energy 35 (2010) 3758–3768.
[28] W. Bujalski, C.M. Dikwal, K. Kendall, J. Power Sourc. 171 (2007) 96–100.
[29] S.P.S. Badwal, K. Foger, Ceramics Int. 22 (1996) 257–265.
[30] S.H. Chan, H.K. Ho, Y. Tian, Int. J. Hydrogen Energy 28 (2003) 889–900.
[31] R.W. Sidwell, W.G. Coors, J. Power Sourc. 143 (2005) 166–172.
[32] S. Kurachi, Y. Mizutani, T. Hiroyama, K. Katsurayama, F. Okada, K. Ukai, in: 24th World Gas Conference, Argentina, 2009.
[33] N. Watanabe, T. Ooe, T. Ishihara, J. Power Sourc. 199 (2012) 117–123.
[34] M. Sorrentino, C. Pianese, J. Fuel Cell Sci. Technol. 6 (2009) 041011–041012.
[35] N. Lutsey, C.-J. Brodrick, T. Lipman, Energy 32 (2007) 2428–2438.
[36] H.C. Maru, S.C. Singhal, C. Stone, D. Wheeler, 1–10 KW Stationary Combined Heat and Power Systems Status and Technical Potential: Independent Review, Report no. NREL/BK-6A10-48265 (2010).
[37] T. Wakui, R. Yokoyama, K.-I. Shimizu, Energy 35 (2010) 740–750.
[38] S. Ghosh, S. De, Energy 31 (2006) 345–363.
[39] D.L. Daggett, United States, Patent No. 20080001038, 2008.
[40] M. Santarelli, M. Cabrera, M. Cali, J. Fuel Cell Sci. Technol. 7 (2010) 021006–021011.
[41] K. Rajashekara, J. Grieve, D. Daggett, Ind. Appl. Magazine IEEE 14 (2008) 54–60.
[42] W. Winkler, H. Lorenz, J. Power Sourc. 106 (2002) 338–343.
[43] J. Van herle, R. Ihringer, N.M. Sammes, G. Tompsett, K. Kendall, K. Yamada, C. Wen, T. Kawada, M. Ihara, J. Mizusaki, Solid State Ionics 132 (2000) 333–342.
[44] Fuel Cells Bull. 2008 (2008) 4.
[45] R. Braun, K. Kattke, ECS Trans. 25 (2009) 291–300.
[46] V. Lawlor, S. Griesser, G. Buchinger, A.G. Olabi, S. Cordiner, D. Meissner, J. Power Sourc. 193 (2009) 387–399.
[47] K. Kendall, Int. J. Appl. Ceram. Technol. 7 (2009) 1–9.
[48] R.J. Kee, H. Zhu, A.M. Sukeshini, G.S. Jackson, Combust. Sci. Technol. 180 (2008) 1207–1244.
[49] W.G. Bessler, in: Fakultät für Chemie und Geowissenschaften, der Ruprecht-Karls-Universität, Heidelberg, 2007.
[50] E. Baur, H. Preis, Z. Elektrochem. 43 (1937) 727–732.
[51] N.Q. Minh, T. Takahashi, Science and Technology of Ceramic Fuel Cells, Elsevier, Amsterdam, 1995.
[52] R.J. Kee, H. Zhu, D. Goodwin. Conference Papers, Proc. Combust. Inst. 30 (2005) 2379–2404.
[53] N.Q. Minh, J. Am. Ceramic Soc. 76 (1993) 563–588.
[54] R.M. Ormerod, ChemInform 34 (2003).
[55] H.-H. Möbius, J. Solid State Electrochem. 1 (1997) 2–16.
[56] K.C. Wincewicz, J.S. Cooper, J. Power Sourc. 140 (2005) 280–296.
[57] J. Thijssen [online], http://www.netl.doe.gov/technologies/coalpower/fuelcells/publications/JT%20Manufacturing%20Study%20Report%20070522.pdf (accessed 05.08.10).
[58] C. Finnerty, David Coimbra, United States, Patent No. 6998187, 2006.
[59] S.-B. Lee, T.-H. Lim, R.-H. Song, D.-R. Shin, S.-K. Dong, Int. J. Hydrogen Energy 33 (2008) 2330–2336.
[60] V. Lawlor, C. Hochenauer, A. Mariani, S. Griesser, S. Kuehn, K. Klein, A.G. Olabi, S. Cordiner, D. Meissner, G. Buchinger, Open Fuel Cells J. 5 (2012) 1–13.
[61] H. Luebbe, J. Rossen, S. Diethelm, J.V. Herle, H. Hofmann, P. Bowen, F. Snijkers, T. Betz, ECS Trans. 25 (2009) 2597–2606.
[62] P. Nehter, J. Power Sourc. 157 (2006) 325–334.
[63] Y. Funahashi, T. Shimamori, T. Suzuki, Y. Fujishiro, M. Awano, Fuel Cells 9 (2009) 711–716.
[64] Y.-S. Chou, J.W. Stevenson, J.S. Hardy, P. Singh, J. Electrochem. Soc. 153 (2006) A1591–A1598.
[65] P. Singh, Z. Yang, V. Viswanathan, J. Stevenson, J. Mater. Eng. Perform. 13 (2004) 287–294.
[66] H. Tuller, Kathy Sahner, United States, Patent No. 20090011316, 2009.
[67] N.R. Quick, Michael Liberman, Michael C. Murray, United States, Patent No. 20020197520, 2002.
[68] P. Sarkar, Rho Hongsang, United States, Patent No. 20050214613, 2005.
[69] P. Sarkar, Lorne Johanson, Rho Hongsang, United States, Patent No. 20060134489, 2006.
[70] R. Zheng, Gary Kovacik, Rho Hongsang, Partho Sarkar, Luis Yamarte, Mark L. Richardson, Patent No. WO/2005/078842, 2005.
[71] T.R. Armstrong, Michael P. Trammell, Joseph A. Marasco, United States, Patent No. 7785747, 2010.
[72] F.F. Lange, Anil V. Virkar, United States, Patent No. 20100173213, 2010.
[73] S. Kuehn, Patent No. WO/2010/066461, 2010.
[74] S. Kuehn, Patent No. WO/2010/066465, 2010.
[75] I. Riess, Solid State Ionics 157 (2003) 1–17.
[76] A. Atkinson, S. Barnett, R.J. Gorte, J.T.S. Irvine, A.J. McEvoy, M. Mogensen, S.C. Singhal, J. Vohs, Nat. Mater. 3 (2004) 17–27.
[77] C. Sun, U. Stimming, J. Power Sourc. 171 (2007) 247–260.
[78] M. Cimenti, J. Hill, Energies 2 (2009) 377–410.
[79] T. Yamaguchi, N. Sammes, Int. J. Hydrogen Energy 36 (2011) 7656–7660.
[80] T. Suzuki, Y. Funahashi, T. Yamaguchi, Y. Fujishiro, M. Awano, J. Fuel Cell Sci. Technol. 5 (2008) 031201–031203.
[81] M.E. Navarro, X.G. Capdevila, M. Morales, J.J. Roa, M. Segarra, J. Power Sourc. 200 (2012) 45–52.
[82] D. Sarantaridis, A. Atkinson, Fuel Cells 7 (2007) 246–258.
[83] H. Monzon, M.A. Laguna-Bercero, Int. J. Hydrogen Energy 37 (8) (2012) 7262–7270.
[84] M. Ettler, H. Timmermann, J. Malzbender, A. Weber, N.H. Menzler, J. Power Sourc. 195 (2010) 5452–5467.
[85] M. Pihlatie, A. Kaiser, M. Mogensen, Solid State Ionics 180 (2009) 1100–1112.
[86] D. Waldbillig, A. Wood, D.G. Ivey, Solid State Ionics 176 (2005) 847–859.
[87] M. Hauth, W. Lerch, K. Konig, J. Karl, J. Power Sourc. 196 (2011) 7144–7151.
[88] R.S. Gemmen, C.D. Johnson, J. Power Sourc. 159 (2006) 646–655.
[89] T. Suzuki, T. Yamaguchi, Y. Fujishiro, M. Awano, J. Power Sourc. 163 (2007) 737–742.
[90] T. Suzuki, B. Liang, K. Hamamoto, T. Yamaguchi, Y. Fujishiro, M. Awano, J. Fuel Cell Sci. Technol. 8 (2011) 061013–061014.
[91] R. De la Torre, V.M. Sglavo, Int. J. Appl. Ceram. Technol. (2012). n/a–n/a.
[92] M. Mori, Y. Liu, T. Itoh, J. Electrochem. Soc. 156 (2009) B1182–B1187.
[93] J.N. Soderberg, L. Sun, P. Sarkar, V.I. Birss, J. Electrochem. Soc. 156 (2009) B721–B728.
[94] T. Suzuki, T. Yamaguchi, Y. Fujishiro, M. Awano, Y. Funahashi, J. Fuel Cell Sci. Technol. 7 (2010) 031005.
[95] Y. Funahashi, T. Shimamori, T. Suzuki, Y. Fujishiro, M. Awano, J. Fuel Cell Sci. Technol. 7 (2010) 021014–021015.
[96] Y. Funahashi, T. Shimamori, T. Suzuki, Y. Fujishiro, M. Awano, J. Power Sourc. 163 (2007) 731–736.
[97] Z.G. Lu, J.H. Zhu, Electrochem. Solid State Lett. 10 (2007) B179–B182.
[98] J.Y. Kim, J.-P. Choi, K. Scott Weil, Int. J. Hydrogen Energy 33 (2008) 3952–3961.
[99] N. Akhtar, K. Kendall, Int. J. Hydrogen Energy 36 (2010) 773–778.
[100] Y. Funahashi, T. Shimamori, T. Suzuki, Y. Fujishiro, M. Awano, T. Araki, J. Fuel Cell Sci. Technol. 7 (2010) 051012–051015.
[101] X. Zhang, B. Lin, Y. Ling, Y. Dong, G. Meng, X. Liu, Int. J. Hydrogen Energy 35 (2010) 8654–8662.
[102] S.C. Singhal, High Temperature Solid Oxide Fuel Cells, Elsevier, Oxford, 2003.
[103] K. Kendall, Int. J. Appl. Ceram. Technol. 7 (1) (2009) 1–9.
[104] K. Kendall, Int. Mater. Rev. 50 (2005) 257–264.
[105] S.H. Jo, P. Muralidharan, D.K. Kim, J. Alloys Compd. 491 (2010) 416–419.
[106] T. Miyashita, J. Mater. Sci. 41 (2006) 3183–3184.
[107] J.S. Ahn, M.A. Camaratta, D. Pergolesi, K.T. Lee, H. Yoon, B.W. Lee, D.W. Jung, E. Traversa, E.D. Wachsman, J. Electrochem. Soc. 157 (2010) B376–B382.
[108] N.M. Sammes, Y. Du, Int. J. Appl. Ceram. Technol. 4 (2007) 89–102.
[109] T. Suzuki, M.H. Zahir, T. Yamaguchi, Y. Fujishiro, M. Awano, N. Sammes, J. Power Sourc. 195 (2010) 7825–7828.
[110] B. Zhu, X.T. Yang, J. Xu, Z.G. Zhu, S.J. Ji, M.T. Sun, J.C. Sun, J. Power Sourc. 118 (2003) 47–53.
[111] K.D. Kreuer, Annu. Rev. Mater. Res. 33 (2003) 333–359.
[112] E. Fabbri, L. Bi, D. Pergolesi, E. Traversa, Adv. Mater. 24 (2012) 195–208.
[113] F. Zhao, C. Jin, C. Yang, S. Wang, F. Chen, J. Power Sourc. 196 (2011) 688–691.
[114] C. Chen, M. Liu, Y. Bai, L. Yang, E. Xie, M. Liu, Electrochem. Commun. 13 (2011) 615–618.
[115] C. Finnerty, David Coimbra, Patent No. WO/2005/057685, 2005.
[116] M.C. Tucker, J. Power Sourc. 195 (2010) 4570–4582.

[117] V. Lawlor, G. Zauner, C. Hochenauer, A. Mariani, S. Griesser, J.G. Carton, K. Klein, S. Kuehn, A.G. Olabi, S. Cordiner, D. Meissner, G. Buchinger, J. Fuel Cell Sci. Technol. 7 (2010) 061016–061017.
[118] T. Yamaguchi, S. Shimizu, T. Suzuki, Y. Fujishiro, M. Awano, Electrochem. Commun. 10 (2008) 1381–1383.
[119] C. Yang, C. Jin, F. Chen, Electrochem. Commun. 12 (2010) 657–660.
[120] R. Campana, R.I. Merino, A. Larrea, I. Villarreal, V.M. Orera, J. Power Sourc. 192 (2009) 120–125.
[121] F. Calise, G. Restucccia, N. Sammes, J. Power Sourc. 195 (2009) 1163–1170.
[122] H. Nakajima, T. Konomi, T. Kitahara, ECS Trans. 25 (2009) 359–368.
[123] K.V. Galloway, N.M. Sammes, J. Electrochem. Soc. 156 (2009) B526–B531.
[124] T. Suzuki, Y. Funahashi, T. Yamaguchi, Y. Fujishiro, M. Awano, Solid State Ionics 180 (2009) 546–549.
[125] P. Sarkar, D. De, H. Rho, J. Mater. Sci. 39 (2004) 819–823.
[126] C.M. Dikwal, W. Bujalski, K. Kendall, J. Power Sourc. 193 (2009) 241–248.
[127] P. Sarkar, L. Yamarte, L. Johanson, ECS Trans. 7 (2007) 603–608.
[128] L.Y.H.R.L.J. Partho Sarkar, Int. J. Appl. Ceram. Technol. 4 (2007) 103–108.
[129] G. Buchinger, P. Hinterreiter, T. Raab, S. Griesser, V. Lawlor, K. Klein, S. Kuehn, W. Sitte, D. Meissner, in: International Conference on Clean Electrical Power, 2007, ICCEP '07, 2007, pp. 444–449.
[130] G. Buchinger, J. Kraut, T. Raab, S. Griesser, V. Lawlor, J. Haiber, R. Hiesgen, W. Sitte, D. Meissner, in: International Conference on Clean Electrical Power, 2007, ICCEP '07, 2007, pp. 450–455.
[131] N. Stelzer, R. Zauner, W. Grienauer, L. Baca, Fabrik der zukunft – Impulsprogramm Nachhaltig Wirtschaften, Berichte aus Energie- und Umweltforschung 69/2006 (2006).
[132] A. Mirahmadi, K. Valefi, Ionics 17 (2011) 767–783.
[133] A. Kawakami, S. Matsuoka, N. Watanbe, T. Saito, A. Ueno, T. Ishihara, N. Sakai, H. Yokokawa, Development of two types of tubular SOFCS at TOTO, in: Advances in Solid Oxide Fuel Cells II: Ceramic Engineering and Science Proceedings, John Wiley & Sons, Inc., 2008, pp. 3–12.
[134] D.I.T. Garcia, Production of Microtubular Solid Oxide Fuel Cells, University of Trento, Italy, 2011. [Thesis].
[135] J. Powell, S. Blackburn, J. Eur. Ceramic Soc. 29 (2009) 893–897.
[136] A. Torabi, T.H. Etsell, P. Sarkar, Solid State Ionics, in press, Corrected Proof.
[137] K. Kikuta, C. Kubota, Y. Takeuchi, Y. Ito, T. Usui, J. Eur. Ceramic Soc. 30 (2009) 927–931.
[138] C. Chen, M. Liu, L. Yang, M. Liu, Int. J. Hydrogen Energy 36 (2011) 5604–5610.
[139] J. Ding, J. Liu, W. Yuan, Y. Zhang, J. Eur. Ceramic Soc. 28 (2008) 3113–3117.
[140] M. Kendall, A Novel Design for a Solid Oxide Fuel Cell, Middlesex University, London, 1993.
[141] T. Suzuki, Y. Funahashi, Z. Hasan, T. Yamaguchi, Y. Fujishiro, M. Awano, Electrochem. Commun. 10 (2008) 1563–1566.
[142] Y.D.N.M. Sammes, Int. J. Appl. Ceram. Technol. 4 (2007) 89–102.
[143] T. Jardiel, B. Levenfeld, R. Jiménez, A. Várez, Ceramics Int. 35 (2009) 2329–2335.
[144] Y. Du, N.M. Sammes, G.A. Tompsett, J. Eur. Ceramic Soc. 20 (2000) 959–965.
[145] R.-h. Song, Dong-ryul Shin, Eung-yong Kim, Harumi Yokokawa, United States, Patent No. 6436565, 2002.
[146] B.-T. Lee, Ho-Yeon Song, Jong-Hee Kim, A.H.M. Esfakur Rahman, Patent No. WO/2008/093995, 2008.
[147] A. Devoe, Mary Trinh, United States, Patent No. 20050000621, 2005.
[148] P. Sarkar, L. Johanson, H. Rho, United States, Patent No. 20030134171, 2003.
[149] X. Tan, W. Yin, B. Meng, X. Meng, N. Yang, Z. Ma, Sci. China Ser. B Chem. 51 (2008) 808–812.
[150] N. Yang, X. Tan, Z. Ma, J. Power Sourc. 183 (2008) 14–19.
[151] N. Droushiotis, U. Doraswami, K. Kanawka, G.H. Kelsall, K. Li, Solid State Ionics 180 (2009) 1091–1099.
[152] G. Kelsall, Patent No. WO/2010/103269, 2010.
[153] M.H.D. Othman, Z. Wu, N. Droushiotis, U. Doraswami, G. Kelsall, K. Li, J. Memb. Sci. 351 (2010) 196–204.
[154] F.D. Grande, A. Thursfield, K. Kanawka, N. Droushiotis, U. Doraswami, K. Li, G. Kelsall, I.S. Metcalfe, Solid State Ionics 180 (2009) 800–804.
[155] N.D. Droushiotis, U. Doraswami, M. Othman, K. Li, G. Kelsall, ECS Trans. 25 (2009) 665–672.
[156] P.T. Torgerson, Richard Dunstan, Mark C. Williams, United States, Patent No. 20080254335, 2008.
[157] P.H. Larsen, Mogens Bjerg Mogensen, Soren Linderoth, Kent Kammer Hansen, Weiguo Wang, United States, Patent No. 7745031, 2010.
[158] A. Laresgoiti Rementeria, Villarreal Sarria, Igor, Rodríguez Martínez, Lide Mercedes Patent No. EP2200115, 2010.
[159] I. Villarreal, M. Rivas, L.M. Rodriguez-Martinez, L. Otaegi, A. Zabala, N. Gomez, M. Alvarez, I. Antepara, N. Arizmendiarrieta, J. Manzanedo, M. Olave, A. Urriolabeitia, N. Burgos, F. Castro, A. Laresgoiti, ECS Trans. 25 (2009) 689–694.
[160] H. Kurokawa, G.Y. Lau, C.P. Jacobson, L.C. De Jonghe, S.J. Visco, J. Mater. Process. Technol. 182 (2007) 469–476.
[161] M. Ettler, Einfluss von Reoxidationszyklen auf die Betriebsfestigkeit von anodengestützten Festoxid-Brennstoffzellen Schriften des Forschungszentrums Jülich Reihe Energie & Umwelt/Energy & Environment, Bochum, University, 2010. [Thesis].
[162] G. Stathis, D. Simwonis, F. Tietz, A. Moropoulou, A. Naoumides, J. Mater. Res. 17 (2002) 951–958.
[163] Y. Zhang, B. Liu, B. Tu, Y. Dong, M. Cheng, Solid State Ionics 180 (2009) 1580–1586.
[164] K.M. Walters, A.M. Dean, H. Zhu, R.J. Kee, J. Power Sourc. 123 (2003) 182–189.
[165] K. Sasaki, Y. Teraoka, J. Electrochem. Soc. 150 (2003) A878–A884.
[166] K. Sasaki, Y. Teraoka, J. Electrochem. Soc. 150 (2003) A885–A888.
[167] G.J. Offer, J. Mermelstein, E. Brightman, N.P. Brandon, J. Am. Ceramic Soc. 92 (2009) 763–780.
[168] E. Ivers-Tiffee, H. Timmermann, A. Leonide, N.H. Menzler, J. Malzbender, in: H.t.A.G. Wolf Vielstich, Arnold Lamm, Harumi Yokokawa (Eds.), Handbook of Fuel Cells – Fundamentals, Technology and Applications (2010), pp. 1–24.
[169] S. Yoon, Y. Kim, S. Kim, J. Bae, J. Solid State Electrochem. 14 (2011) 1793–1800.
[170] Pirelli_&_C_SpA [online], http://www.pirellilabs.com/web/material_innovation/collaborations/alberta_research_council/default.page (accessed: 18–10).
[171] N. Bessette [online], http://www.hydrogen.energy.gov/pdfs/review09/fc_28_bessette.pdf (accessed 22.05.10).
[172] N. Bessette [online], http://www.netl.doe.gov/publications/proceedings/06/seca/pdf/BessettePhilly%202006%20SECA%20Acumentrics-Pub.pdf (accessed 22.05.10).
[173] N. Bessette [online], http://www.netl.doe.gov/publications/proceedings/04/seca-wrkshp/acumentrics%20-%20bessette.pdf (accessed: 22 May).
[174] Acumentrics Inc.. http://www.acumentrics.com/products-power-generators.htm (accessed).
[175] C. Finnerty, R. Cunningham, R. Ormerod, Catal. Lett. 66 (2000) 221–226.
[176] K. Kendall, C.M. Dikwal, W. Bujalski, ECS Trans. 7 (2007) 1521–1526.
[177] F. Calise, G. Restucccia, N. Sammes, J. Power Sourc. 196 (2011) 301–312.
[178] G. Buchinger, P. Hinterreiter, T. Raab, S. Griesser, R. Claassen, D.P. Claassen, W. Sitte, D. Meissner, J. Fuel Cell Sci. Technol. 3 (2006) 280–283.
[179] K. Kendall, M. Slinn, J. Preece, J. Power Sourc. 157 (2006) 750–753.
[180] Z. Zhan, S.I. Lee, J. Power Sourc. 195 (2010) 3494–3497.
[181] M. Yano, A. Tomita, M. Sano, T. Hibino, Solid State Ionics 177 (2007) 3351–3359.
[182] N. Akhtar, S.P. Decent, K. Kendall, J. Power Sourc. 195 (2010) 7796–7807.
[183] N. Akhtar, S.P. Decent, K. Kendall, J. Power Sourc. 195 (2010) 7818–7824.
[184] S.D. Ebbesen, J. Høgh, K.A. Nielsen, J.U. Nielsen, M. Mogensen, Int. J. Hydrogen Energy 36 (2011) 7363–7373.
[185] M.A. Laguna-Bercero, R. Campana, A. Larrea, J.A. Kilner, V.M. Orera, J. Electrochem. Soc. 157 (2010) B852–B855.
[186] P. Mardilovich, Herman, Gregory S., Beatty, Christopher, O'neil, James, Champion, David, United States, Patent No. 20040202918, 2004.
[187] K. Kendall, C. Dikwal, ECS Trans. 25 (2009) 899–906.
[188] B.R. Roy, N.M. Sammes, T. Suzuki, Y. Funahashi, M. Awano, J. Power Sourc. 188 (2009) 220–224.
[189] A. Mohammadi, J. Pusz, A.L. Smirnova, N.M. Sammes, ECS Trans. 7 (2007) 1409–1418.
[190] B.R. Roy, N.M. Sammes, ECS Trans. 25 (2009) 907–916.
[191] S. Hashimoto, H. Nishino, Y. Liu, K. Asano, M. Mori, Y. Funahashi, Y. Fujishiro, J. Fuel Cell Sci. Technol. 5 (2008) 31205–31208.
[192] M.F. Serincan, U. Pasaogullari, N.M. Sammes, J. Power Sourc. 195 (2010) 4905–4914.
[193] S.R. Bishop, K. Duncan, E.D. Wachsman, ECS Trans. 1 (2006) 13–21.
[194] D. Cui, L. Liu, Y. Dong, M. Cheng, J. Power Sourc. 174 (2007) 246–254.
[195] A. Mariani, in: EUA4X#19 Conference MASCOT06, IAC-CNR, Rome Italy, 2006, pp. 1–10.
[196] D. Cui, M. Cheng, J. Power Sourc. 192 (2009) 400–407.
[197] L. Blum, S.M. Groß, J. Malzbender, U. Pabst, M. Peksen, R. Peters, I.C. Vinke, J. Power Sourc., in press, Corrected Proof.
[198] S. Griesser, G. Buchinger, T. Raab, D.P. Claassen, D. Meissner, J. Fuel Cell Sci. Technol. 4 (2007) 84–87.
[199] V. Lawlor, J. Fuel Cell Sci. Technol. 9 (2012) 024501–024504.
[200] R.S. Gemmen, M.C. Williams, K. Gerdes, J. Power Sourc. 184 (2008) 251–259.
[201] V.A.C. Haanappel, M.J. Smith, J. Power Sourc. 171 (2007) 169–178.
[202] Q.-A. Huang, R. Hui, B. Wang, J. Zhang, Electrochim. Acta 52 (2007) 8144–8164.
[203] H. Nakajima, T. Kitahara, T. Konomi, J. Electrochem. Soc. 157 (2011) B1686–B1692.
[204] G. Buchinger, T. Raab, S. Griesser, V. Lawlor, S. Potzmann, S. Kuehn, K. Klein, D. Mootz, H. Hofbauer, W. Sitte, D. Meissner, in: EFC2007, ASME, Rome, 2007. EFC2007-39033.